Serotonin selectively modulates visual responses of object motion detection in *Drosophila*

David J. Bertsch[1], Lesly M. Palacios Castillo[1], and Mark A. Frye[1]

[1]Department of Integrative Biology and Physiology, University of California, Los Angeles, Los Angeles, CA 90025-7239, USA

Correspondence: frye@ucla.edu

Abstract

Serotonin (5-HT) is a hormonal messenger that confers state-level changes upon the nervous system in both humans and flies. In *Drosophila*, lobula columnar (LC) cells are feature-detecting neurons that project from the optic lobe to the central brain, where each population forms an anatomically-distinct glomerulus with heterogeneous synaptic partners. Here, we investigated serotonin's effect on two LC populations with different 5-HT receptor expression profiles. Receptor expression does not predict neuromodulatory effects: LC15 expresses inhibitory 5-HT1A and 5-HT1B receptors, yet serotonin increases the amplitude of calcium responses to visual stimuli. LC12 expresses inhibitory 5-HT1A and excitatory 5-HT2A receptors, yet serotonin application does not influence visual responses. Serotonin targets select visual response properties, potentiating LC15 responses to a motion-defined bar and normalizing responses across bar velocity, but has no influence on contrast sensitivity. Serotonin does not significantly facilitate LC15 responses in postsynaptic dendrites, only in the presynaptic terminals of the glomerulus, which suggests that the neuromodulatory effects are strongest in the central brain. Connectomics confirms that LC12 and LC15 share neither presynaptic inputs nor postsynaptic outputs in the central brain. The wiring diagram shows no synaptic interactions between the LC15 circuit and major serotonergic 5-HTPLP neurons, nor to other serotonergic neurons of the central brain, suggesting that endogenous 5-HT acts via paracrine transmission on non-serotonergic pathways. Lobula- and glomulus-specific GABAergic and glutamatergic inhibitory partners, positioned to filter visual stimuli, are putative 5-HT targets. These results provide a comparative framework for the neuromodulatory mechanisms involved in visual processing.

New & Noteworthy

How does neuromodulatory state affect visual feature detection? In the present work, we demonstrate highly specific facilitated visual responses of object-detecting neurons after serotonin bath application in *Drosophila*. Serotonin potentiates motion-defined bar responses in object-detecting LC15 neurons and normalizes responses to translating bars of increasing velocity in presynaptic axon terminals. Our calcium imaging extends what is known about extra-synaptic neuromodulation in the visual system and shows that serotonin heightens visual processes that inform object-specific behavior.

Keywords: *Drosophila*; neuromodulation; sensory processing; serotonin; visual system

Introduction

Visual animals must extract object information from a complex, changing external environment while receiving internal physiological cues to produce context-specific behavior. Endogenous release of signaling molecules communicate state-dependent changes in all animals yet we understand neither how these neuromodulators transform visual information as it enters the central brain nor how they reconfigure the hard-wired and numerically-limited circuits of the brain to create flexible state-dependent behavior (Alekseyenko and Kravitz 2014). An important class of neuromodulatory peptides is the biogenic monoamines which impart remarkable flexibility to both vertebrate and invertebrate neural networks (Nässel 2025). The biogenic amines activate G protein-coupled receptors (GPCRs) on target cells and include dopamine (DA), serotonin (5-HT), tyramine (TA), norepinephrine (NE) and the invertebrate analog, octopamine (OA) (Blenau and Baumann 2001; El-Kholy et al. 2015; Evans and Maqueira 2005; Monastirioti 1999). Serotonin (5-hydroxytryptamine, 5-HT) is a pleiotropic neurotransmitter and neurohormone that mediates learning and memory, sleep, feeding, aggression, arousal, courtship, swarming behavior in locusts, and locomotion as well as various developmental or physiological processes including critical period plasticity in both vertebrates and invertebrates (Anstey et al. 2009; Becnel et al. 2011; Dierick and Greenspan 2007; Johnson et al. 2009, 2011; Majeed et al. 2016; Mallick et al. 2024; Pooryasin and Fiala 2015; Qian et al. 2017; Sitaraman et al. 2008; Vleugels et al. 2014). Importantly, 5-HT has been implicated in enhancing gain control in the glomeruli of the olfactory antennal lobe (Dacks et al. 2009; Suzuki et al. 2020; Zhang and Gaudry 2016), and for enhanced visual responses by lamina class L2 in response to OFF objects (i.e. objects darker than the background) (Sampson et al. 2020).

The genetically-tractable fly *Drosophila melanogaster* has been used for decades to understand visual processing and neuromodulatory control of behavior. Detailed reviews have summarized how the anatomy and physiology of the optic lobe relates to visual information processing (Borst et al. 2020; Fischbach and Dittrich 1989; Ryu et al. 2022; Zhu 2013). In brief, luminance changes in the environment are detected by photoreceptors in the retina (R1-R6) before being transmitted downstream to the optic lobe. The optic lobe is composed of four neuropils: the lamina, medulla, lobula, and lobula plate. Each neuropil shows anatomically-distinct ‘horizontal’ processing layers and retinotopic arrays of ‘vertical’ columns where luminance signals are processed for directional motion, features, or color. Columnar signals are spatially integrated by visual projection neurons (VPNs) that send axons to higher brain areas. The innermost neuropil of the optic lobe, the lobula (Lo), houses a class of VPNs called lobula columnar (LC) cells. The LCs include 22 neural populations that encode select visual features of relevant objects in the fly’s environment (Klapoetke et al. 2022; Wu et al. 2016). Each LC type is made up of numerous clones of similar morphology that tile the visual field. Dendrites integrate synaptic inputs across a set of visual columns, the number of which varies for each LC type, and project axons to the central brain where the terminals of all members of a given type converge with postsynaptic neurons within an anatomically-distinct optic glomerulus (OG) in the anterior or posterior ventrolateral protocerebrum (AVLP, PVLP) (Otsuna and Ito 2006; Panser et al. 2016; Strausfeld 1976; Strausfeld and Okamura 2007). LC12 and LC15 both respond to translating bars, which

are highly engaging to a flying fly as they represent landscape features moving against the visual surroundings (Fox et al. 2014). Bars may be defined by luminance (darker or brighter than the visual surroundings) or by optical disparities generated by translational cues relative to the stationary ground (i.e. motion). Neither LC12 nor LC15 respond to wide-field motion (square grating period 17.6°), and both types have their postsynaptic dendrites in Lo layers 2 and 4. It has been demonstrated using two-photon calcium imaging that LC cells can be measured individually in the Lo whereas the population of axon terminals can be measured collectively at the terminal OG (Aptekar et al. 2015; Keleş and Frye 2017). Within the OG, LC12 and LC15 axon terminals make excitatory and inhibitory synapses with other cell types. We have previously shown that both LC12 and LC15 show modulation by bath application of an octopamine agonist (Städele et al. 2020). LC responses to local features have previously been measured using single-cell or pan-neuronal imaging and functionally grouped (Klapoetke et al. 2022; Turner et al. 2022). In one report, LC15 was grouped by strong responses to moving objects, with weak responses to looming objects, whereas LC12 was grouped by its strong responses to looming and preference for OFF over ON contrast polarity (Klapoetke et al. 2022). A second study placed both LC12 and LC15 in the same group defined by strong responses to vertical bars as well as medium and large moving spots, plus some looming sensitivity (Turner et al. 2022). Disparities in LC response classification could be due to the specific approach used, or by higher order neuromodulation of complex feature detectors.

We explored the effects of 5-HT on LC responses in the optic lobe and optic glomeruli of the central brain of *Drosophila melanogaster* using pharmacology, single-cell intersectional genetics, connectomics, and two-photon calcium imaging. To mimic the effects of volumetric neurohormonal release, we bath-applied serotonin HCl in *Drosophila* saline while performing two-photon calcium imaging. Imaging revealed that 5-HT bath application enhances LC15 responses to motion-defined vertical bars. Although the dendrites showed stronger Ca^{2+} responses, they did not show a significant potentiation after 5-HT; this potentiation effect is strongest in the axon terminals of the OG in the PVLP. We next presented OFF bars moving at different speeds and observed that 5-HT significantly increases the LC15 glomerular response to faster velocities, effectively normalizing velocity sensitivity. To determine if this serotonergic potentiation is a general phenomenon among bar-sensitive feature detectors, we showed the same bar stimuli while imaging the LC12 glomerulus and did not observe any modulatory change. Using the synaptic connectome (Dorkenwald et al. 2024), we detail LC-specific GABAergic inhibitory neurons that display reciprocal innervation of the LCs and could mediate glomerular potentiation. Both VPN types respond to translating bar stimuli but only LC15 shows potentiated Ca^{2+} responses to specific objects after 5-HT bath application. Our data support the hypothesis that serotonergic potentiation occurs within axon terminals of the VLP and the two LC types respond to the neuropeptide in ways that are likely determined by their specific synaptic partners rather than their 5-HTR expression profile.

Materials and Methods

Fly stocks

Drosophila melanogaster were maintained on a standard cornmeal and molasses-based agar media with a 12:12 hour light/dark cycle at room temperature (22-25°C) in 40 ml vials. Only 3-5

day old adult females were used for experimentation. To genetically target LC neurons we exclusively used split-GAL4 driver lines because of their high specificity for the respective class of neurons. OL0042B was the driver line used to target LC15 and OL0007B to target LC12 (Wu et al. 2016). These flies were crossed with virgin females expressing UAS-GCaMP6f and the progeny were used for experiments (Chen et al. 2013).

Animal preparation

Imaging experiments were performed between ZT0–14, although time of day was not a factor in our experimental design or analysis. Female flies were anesthetized at 4°C on a cold plate and mounted to a custom 3D printed fly holder using ultraviolet glue (Form3 SLA printer, FormLabs; Dreve Fotoplast gel, Audiology Supplies, 44811). The fly's legs were immobilized with low melting point beeswax to eliminate interference with recordings and visual stimulation. Fine forceps (Dumont, #5SF, Fine Science Tools) were used to remove the cuticle on the posterior surface of the fly's head to expose the right optic lobe in the region of the lobula and VLP. We severed muscles 1 and 16 to reduce brain movements. This approach has previously been used in our laboratory (Hardcastle et al. 2021; Städele et al. 2020).

Pharmacology and bath perfusion

D. melanogaster saline was composed of ultrapure water (18.3 MU, Millipore) and (in mM): 103 NaCl, 3 KCl, 1.5 $CaCl_2$, 4 $MgCl_2$, 26 $NaHCO_3$, 1 NaH_2PO_4, 10 trehalose, 10 glucose, 5 TES, 2 sucrose, pH 7.0 - 7.25. Serotonin HCl (Sigma Aldrich, cat# H9523) stock solutions were stored at 20°C in small quantities and diluted in *D. melanogaster* saline to the final concentration of 100 µM. All 5-HT solutions were kept away from light. Measurements were taken after a 10 minute wash-in. During two-photon imaging, the brain was continuously perfused with freshly prepared extracellular saline or 5-HT HCl solution or at 1.5 ml/min via a computer-controlled six channel valve controller (VC-6, Warner Instruments) and a custom built gravity-drip perfusion system. Bath temperature was kept at 20°C with an inline-solution heater (SC-20, Warner Instruments) and a temperature controller (TC-324, Warner Instruments).

Two-photon calcium imaging

LC neurons were imaged at 920 nm using a Ti:Sapphire pulse laser (Chameleon Vision, Coherent, Santa Clara, CA) controlled by SlideBook (Version 6, 3i, Boulder, CO). We imaged with a 20x water-immersion objective (W Plan-Apochromat, 1.0 DIC, Zeiss) with three layers of blue filter (Indigo, Rosco, No. 59) to reduce bleed-through from the LED arena to the photomultipliers. Single plane images were taken at 7.0-10.0 frames/s with each frame at a x-y pixel resolution ranging from 150 x 256 to 168 x 212 and 0.2 to 0.3 mm pixel spacing. Images and external stimulations were synchronized a posteriori using frame capture markers (TTL pulses output from Slidebook) and stimulus events (analog outputs from the LED display controller) sampled with a data acquisition device (DAQ) (PXI-6259, NI) at 10 kHz. The DAQ interfaced with MATLAB (R2020a, MathWorks) via rack-mount terminal block (BNC-2090, NI). To record population responses of a given LC type, GCaMP6f responses were recorded in the LC output glomeruli where all terminals merge together. To record activity of single LC neurons, GCaMP6f responses were collected at different z-planes from individual dendrites in the lobula.

Visual stimulation

Visual stimuli during two-photon imaging were presented on a cylindrical LED arena (Reiser and Dickinson 2008). The arena was composed of 4 rows and 12 columns of 8 x 8 LED dot matrix panels (470nm, Dongguan Houke Electronic, 12088-AB). The LED display covered ±108 of the visual field in the horizontal, and ±35 in the vertical dimension. Each pixel subtended 2.2° on the fly's retina at the visual equator. The display had a maximum intensity of ~0.11 μW m^{-2} (recorded at the fly's position) at the spectral peak of 460 nm (full width at half maximum: 243 nm). Stimuli were generated and controlled using custom Matlab scripts.

In Figure 3Bii, Weber contrast is calculated by subtracting the light intensity of the object from the background and dividing by the background intensity.

Two-photon image analysis

Recorded imaging data was exported from SlideBook as 16-bit tiff image stacks and analyzed offline using custom written Matlab scripts. Images were corrected for motion artifacts and ROI selection was performed using a custom toolbox (Hardcastle et al. 2021) (https://github.com/bjhardcastle/SlidebookObj). The ROI selection process was performed for each experimental video and identical for all recordings. Manually drawn ROIs were selected in accord with the anatomical region that was recorded. For glomerular recordings, a single ROI mask encompassed the whole glomerulus. For the dendrite recordings, the Ca^{2+} activity appeared as small fluorescent dots (lobula neurons perpendicular to the imaging plane) or small lines (parallel to the imaging plane). A toolbox function constructs an activity frame image (mean fluorescent intensity per pixel recorded during stimulus trials, subtracted by the mean of all extra-trial frames). All dendrites in frame that had a positive correlation between activity and the stimulus presentation were kept as individual ROIs. For every pixel in this ROI mask, the mean and standard deviation were calculated for the full time series.

Fluorescence quantification

A time series was generated by calculating the mean fluorescence intensity of pixels within the ROI in each frame (F_t). These mean values were then normalized to a baseline value as

$$\Delta F/F_0 = (F_t - F_0)/F_0$$

where F_0 was the mean of F_t during the 0.5 s preceding stimulus onset. To compute average time series across preparations with small variations in TTL synchronization, traces were resampled using linear interpolation. This procedure did not cause any detectable change in the original data.

The cumulative integral of each $\Delta F/F_0$ trace was obtained using the *cumtrapz* function in Matlab. The discrete integration of the GCaMP fluorescent intensity change over time is defined as

$$\int_0^t f(\Delta F/F_0)\, dx$$

where the integrated Ca^{2+} measurement is the total area under the curve measured at the end of the stimulus period.

FlyWire connectome analysis

We exported synaptic connectivity and neural morphology from the FlyWire connectome, using the fafb (v783) dataset (Dorkenwald et al. 2024). The EM reconstruction in v783 uses a coordinate system which is reversed from the fly's anatomy, therefore the right optic lobe is labelled as the left hemisphere throughout the dataset. We used the following queries to generate data for Figure 6, and Tables 1-6.

- cell_type == LC15 && side == left
- cell_type == LC12 && side == left
- cell_type == 5-HTPLP01 && side == left
- nt_type == SER && output_neuropil == PVLP_L

Individual neuron IDs as well as the individual cells within the groups above were used in pathway analysis to assemble Figure 6. Cell type groups were analyzed for neurotransmitter profile, input and output neuropils, synaptic weight, and major upstream and downstream partners, presented in Tables 1-6.

Results

We generated a set of visual stimuli to elicit responses in the two feature detectors. To assess figure-ground discrimination, a hallmark of some LCs, we used a 'motion-defined' bar composed of a narrow vertical bar that is randomly textured similar to the wide-field (WF) background, and thereby indiscriminable by contrast or luminance but rather only when it moves relative to the background (Theobald et al. 2008). The motion-defined bar stimulus is highly engaging, stimulating saccadic pursuit in flight (Mongeau and Frye 2017), and strongly activates high frequency sensitive T2a and T3 cells upstream of the LCs (Frighetto and Frye 2023), but activates low frequency directional motion detectors T4 (ON edge-motion) and T5 (OFF edge-motion) less strongly (Keleş et al. 2019).

We tested vertical motion-defined bars on stationary or moving backgrounds (Figure 1). We also tested a solid 'luminance-defined' bright (light-ON) or dark (light-OFF) bar on a uniform midlevel background. We tested bars of various luminance levels moving from the midline to the periphery at a constant speed (Figure 3). We tested OFF bars translating at different velocities (Figure 4) or cardinal motion directions (data not shown). We investigated the effects of bath-applied 5-HT on LC15, which increased the LC15 response to motion-defined bars translating across a stationary random texture background.

We performed calcium imaging in both the LC15 dendritic arbors and OG in the central brain (Figure 1Ai pink boxes, and inset). We targeted LC15 using the split-gal4 line OL0042B to drive expression of the calcium indicator GCaMP6f (Figure 1Aii) (Chen et al. 2013; Wu et al. 2016). Calcium imaging was performed in the right hemisphere of head-fixed flies (Figure 1Bi). We actively perfused temperature-controlled *Drosophila* saline throughout the duration of the experiment before switching the perfusate to 100 μM of 5-HT hydrochloride dissolved in *Drosophila* saline. Only flies that showed consistent responses to repeated stimuli in the control condition progressed to the 5-HT experimental condition and were included for analysis. Visual stimuli were presented on a curved LED panel display that covers 216° in azimuth (Figure 1Bii)

(Reiser and Dickinson 2008). The anatomy of the LCs are shown in relation to the 5-HTPLP neuron (cyan) that provides 5-HT to the PVLP on the right hemisphere. The 5-HTPMP neurons (black) are also shown but do not innervate the PVLP (Figure 1Biii).

5-HT potentiates object motion responses by LC15

We displayed the same visual scene with four "figure-ground" stimulus conditions, randomly shuffled (Figure 1Ci). The first condition presents the WF moving rightward at 22°/s. The second condition presents the motion-defined vertical bar moving at 22°/s over the stationary WF. The third condition is a motion-defined bar held stationary +55° on azimuth while the WF background moves rightward at 22°/s. The fourth condition presents the bar moving opposite the background, both at 22°/s.

Figure 1Ci depicts the visual patterns as presented on the LED display (top) and the trajectory of the visual stimuli (bottom). Bath application of 5-HT was sufficient to cause a significant increase in the LC15 glomerular responses to a motion-defined bar over a stationary broadband background (Figure 1Cii). However, if the background was moving counter-directional beneath the bar, there was neither a response nor influence of 5-HT. Similarly, LC15 did not respond to a stationary motion-defined bar (+55°) defined by the rotation of the WF background behind it (Figure 1Cii), nor the broadband WF stimulus alone, and 5-HT had no effect (Figure 1Cii). A robust change in the glomerular responses is observable within the single trial responses after 5-HT bath application (Figure 1Ciii). We averaged the trial responses for each fly (Figure 1Civ), and observed a large degree of inter- and intra-animal variability. We lastly examined the effect size (post-5-HT subtracted from pre-5-HT) change for each animal between conditions, sorted by the magnitude of the change (Figure 1Cv). The effect size raster shows that the potentiation is confined to the stimulus that elicited visual responses from LC15, and the strength of the 5-HT effect is animal-specific.

We next tested whether the 5-HT application caused a tonic baseline potentiation of LC15 Ca^{2+} activity, which would be manifested by an increase in the mean fluorescence, F, but did not observe a significant change (saline = 26.0 ±21.0F; 5-HT = 25.5 ±20.6F) (Figure 1D). It was only during the acute presentation of the bar stimulus that we observed significant changes in both the maximum $\Delta F/F_0$ response (Figure 1E) and the time-integrated Ca^{2+} response (Figure 1F). We did not observe a significant change in the onset delay of visual responses, measured by time to half-max (Figure 1G), although there was considerable variability between preparations. These results indicate that 5-HT acts specifically upon the object detection gain of LC15, rather than on baseline excitation.

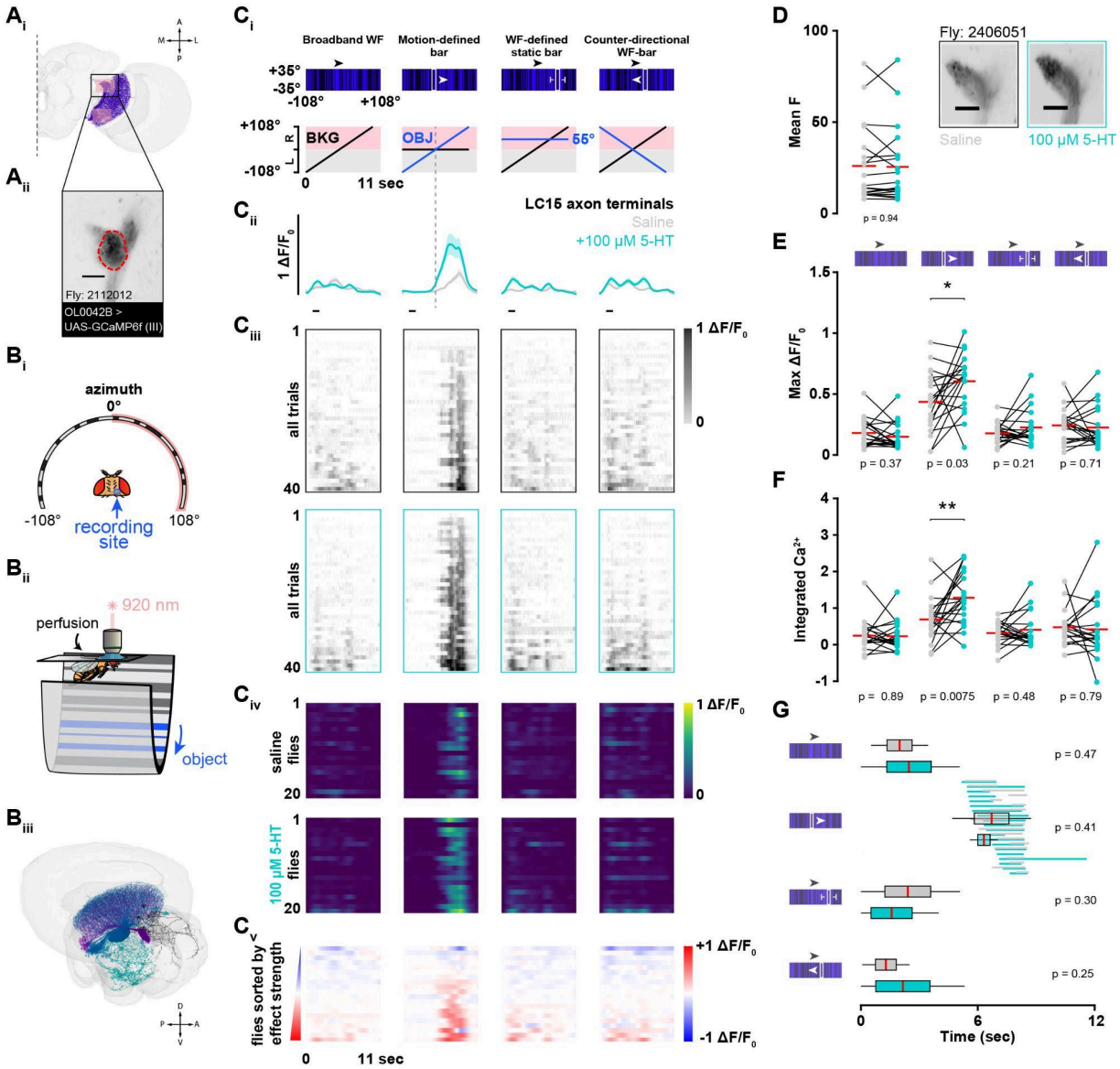

Figure 1. The LC15 glomerular response to a motion-defined bar is potentiated by 5-HT when the background is stationary

(Ai) LC15 cells (purple) in the right hemisphere. The two pink boxes highlight the recording sites: glomerulus of population axon terminals (top box) and individual dendritic projections (bottom box).

(Aii) Two-photon fluorescent image of z-axis projection showing the glomerulus of LC15 cells. The red dotted line defines the region of interest. Scale bar, 25 µm.

(Bi) Cartoon of head-fixed preparation presented with visual stimuli from below using a wrap-around LED display that extends +/- 108° in azimuth. All recordings were collected from the right hemisphere. Not drawn to scale.

(Bii) Schematic showing the two-photon imaging preparation, with 20x water immersion lens. Temperature-controlled *Drosophila* saline was perfused into the preparation for the duration of the experiment.

(Biii) LC15 (purple) and LC12 (blue) do not directly synapse with 5-HTPLP neurons (cyan) in the right hemisphere but likely receive 5-HT through paracrine release into the AVLP and PVLP. Projections from 5-HTPMP are shown in black. Reconstruction generated using FlyWire.ai (Dorkenwald et al. 2024).

(Ci) Schematic illustrating the visual stimulus presented on the LED display (top) and the motion trajectory of object (OBJ) or background (BKG) (bottom).

(Cii) Mean GCaMP6f signal from the LC15 axon terminals (±SEM shading) before (gray) and after 100 μM 5-HT (cyan). The horizontal scale bar (black) represents 1 second.
(Ciii) $\Delta F/F_0$ response raster plots displaying individual trials before and after 100 μM 5-HT (cyan). Two repeats of each stimulus were shown to each animal (N = 20, n = 40). The trial responses are sorted by increasing peak $\Delta F/F_0$ response.
(Civ) $\Delta F/F_0$ response raster plots displaying mean animal responses before (top) and after 100 μM 5-HT (bottom) (N = 20). Flies 1-20 (rows) are sorted the same in the pre-5-HT (top) and post-5-HT (bottom) condition rasters.
(Cv) Mean change in effect size rasters of LC15 glomerular GCaMP6f responses for each animal in the saline and 5-HT conditions. Animals (row) are sorted by increasing effect size strength.
(D) Pairwise comparison of mean fluorescent intensity in the LC15 glomerulus before (gray) and after 100 μM 5-HT (cyan). Horizontal red lines correspond to the population means. Two-tailed paired t-test, N = 20. Insert: average frames of LC15 fluorescence intensity from a single animal before (gray) and after 100 μM 5-HT (cyan). Scale bar, 25 μm.
(E) Pairwise comparison of maximum $\Delta F/F_0$ responses in the LC15 glomerulus before (gray) and after 100 μM 5-HT (cyan). Two-tailed paired t-test, N = 20.
(F) Pairwise comparison of integrated Ca^{2+} responses in the LC15 glomerulus before (gray) and after 100 μM 5-HT (cyan). Two-tailed paired t-test, N = 20.
(G) Pairwise comparison of time to half-max (sec) for LC15 glomerular responses before (gray) and after 100 μM 5-HT (cyan). Two-tailed paired t-test, N = 20. The horizontal lines behind the box plots in the motion-defined bar condition indicate the time period from the half-max to the maximum $\Delta F/F_0$ responses for each animal before (gray) and after 100 μM 5-HT (cyan).

5-HT acts selectively on the presynaptic cell compartment - activating terminals not dendrites

To localize the site of gain modulation by 5-HT, we imaged visual responses in the postsynaptic dendrites in the lobula, reasoning that a change in gain of columnar inputs would modify the amplitude of GCaMP responses in the dendrites. Absence of 5-HT modulation would highlight compartment-specific feature computations and implicate central brain mechanisms acting within the axonal optic glomerulus. We first imaged dendritic responses in the lobula to the motion-defined bar stimuli (Figure 2Ai). LC15 cells are retinotopically-arranged in the lobula and ROIs were drawn around the same posterior region of dendrite branches across preparations (see Methods). Although the visual responses were qualitatively similar in both cell compartments, i.e. largest response was to bar motion across the stationary ground (Figure 2A), we found no 5-HT potentiation in the LC15 dendrites (Figure 2Aii). Some individual dendrites in some individual trials displayed strong Ca^{2+} activity in response to the movement of the WF background (Figure 2A, columns one, three, and four). This is most likely due to phase locking of small-field responses to the spatial variation contained in the stimulus pattern, which is spatially averaged in the glomerular $\Delta F/F_0$ traces (Figure 1Cii). Note that visually activated GCaMP signals are much larger in a small group of dendrites than in the full population of axon terminals, which is also due to spatial averaging of time-shifted retinotopic terminals in the glomerulus. Unlike in the glomerulus (Figure 1), 5-HT did not modulate any of the visual response parameters we measured in the dendrites (Figure 2A-E), with the exception that some additional dendrites were recruited thereby increasing the number of ROIs collected in the post-5-HT condition (n_{pre}= 133, n_{post} = 168). But, none of these measures were significant. These results suggest that 5-HT potentiation of LC15 responses is localized to the subcellular domain of the axon terminals within the glomerulus, where the individual LC15 clones converge and can be innervated by other circuits before conveying information to downstream pathways.

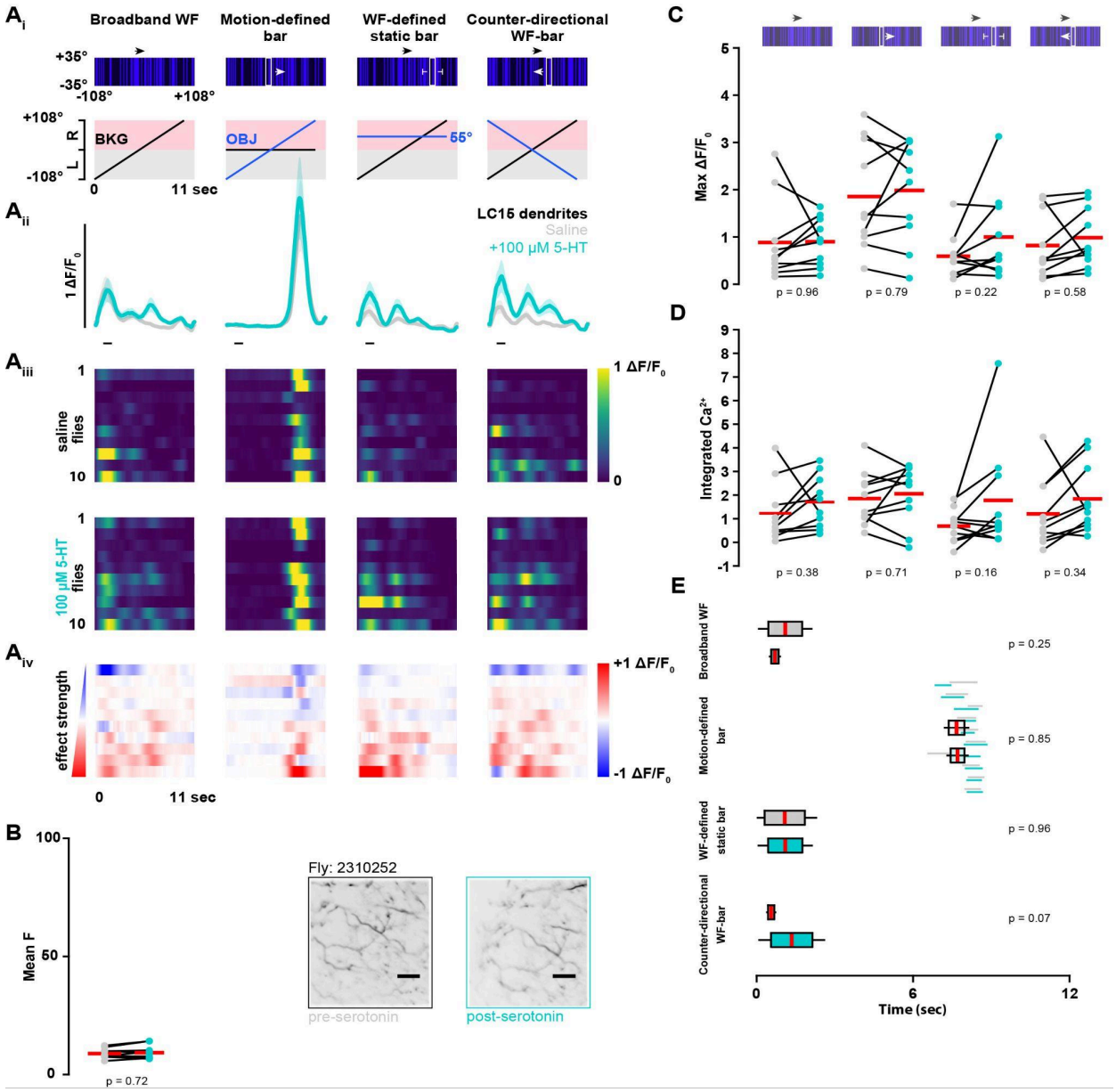

Figure 2. The LC15 dendrites do not show potentiated responses after 5-HT bath perfusion

(Ai) Schematic illustrating the visual stimulus presented on the LED display (top) and the motion of the visual feature elements over time (bottom).

(Aii) Population mean GCaMP6f signal from the LC15 dendrites (±SEM shading) before (gray) and after 100 μM 5-HT (cyan). The vertical scale bar (black) represents 1 $\Delta F/F_0$. The horizontal scale bar (black) represents 1 second.

(Aiii) $\Delta F/F_0$ response raster plots displaying mean animal responses before (top) and after 100 μM 5-HT (bottom) (N = 10). Flies 1-10 (rows) are sorted the same in the pre-5-HT (top) and post-5-HT (bottom) condition rasters.

(Aiv) Mean change in effect size rasters of LC15 dendritic GCaMP6f responses for each animal. Animals (row) are sorted by increasing effect size strength.

(B) Pairwise comparison of mean fluorescent intensity in the LC15 dendrites before (gray) and after 100 μM 5-HT (cyan). Horizontal red lines correspond to the population means. Two-tailed paired t-test. Mean time lapse between pre- and post- conditions = +38 minutes. Insert: average frames of LC15 fluorescence intensity from a single animal before (gray) and after 100 μM 5-HT (cyan). Scale bar, 25 μm.

(C) Pairwise comparison of maximum $\Delta F/F_0$ responses in the LC15 dendrites before (gray) and after 100 μM 5-HT (cyan). Two-tailed paired t-test, N = 10.
(D) Pairwise comparison of integrated Ca^{2+} responses in the LC15 dendrites before (gray) and after 100 μM 5-HT (cyan). Two-tailed paired t-test, N = 10.
(E) Pairwise comparison of time to half-max (sec) for LC15 dendrite responses before (gray) and after 100 μM 5-HT (cyan). Two-tailed paired t-test, N = 10. The horizontal lines behind the box plots in the motion-defined bar condition indicate the time period from the half-max to the maximum $\Delta F/F_0$ responses for each animal before (gray) and after 100 μM 5-HT (cyan).

5-HT acts selectively on bar motion responses - does not modulate responses to varying object luminance

The directional motion vision system is split into ON and OFF subsystems (Maisak et al. 2013), whereas feature detection pathways of the lobula so far studied are ON-OFF responsive (Keleş and Frye 2017; Städele et al. 2020), and LCs receive inputs from both systems (Behnia et al. 2014; Joesch et al. 2010; Strother et al. 2014). We therefore sought to test whether 5-HT selectively modulated ON or OFF selective pathways to LC15. We collected Ca^{2+} responses from the lobula dendrites (Figure 3C) as well as the central brain axon terminals (Figure 3H) while presenting a 8.8° x 70° vertical bar of eight different luminance values, set against a fixed luminance uniform background. The bar moved at 22°/s across the right side of the panel display (Figure 3A), with varying Weber contrast in randomized order (Figure 3Bi,Bii).

LC15 dendrites are contrast sensitive, but do not significantly prefer either polarity (Figure 3Ci), and these responses show no significant modulation by 5-HT in either individual or populations measures of effect strength, mean baseline fluorescence, max GCaMP amplitude, time-integrated GCaMP response, or onset delay (Figure 3C-G). The tonic level of GCaMP fluorescence (mean F) was higher in the glomerulus (control: 27 ±21F; 5-HT: 26 ±19F) than in the dendrites (control: 9.5 ±2.2F; 5-HT: 10.1 ±2.6F) but this is to be expected from averaging across all members of the cell class in volumetric imaging. Unlike the figure-ground stimulus (Figure 1), 5-HT did not modulate responses to object contrast in the axon terminals of the optic glomerulus (Figure 3H). Neither were any of the measured parameters significantly modulated (Figure 3I-L).

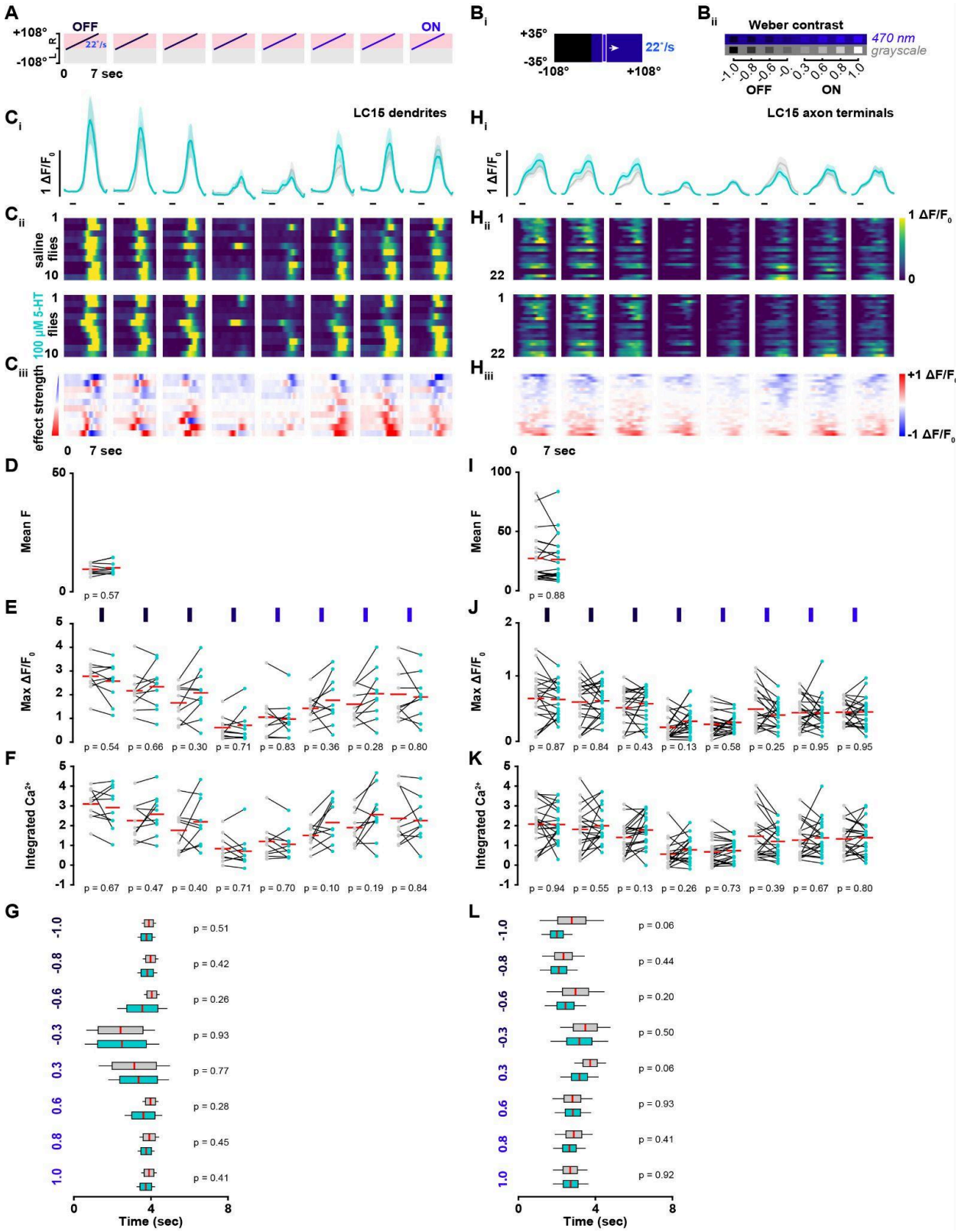
A
OFF
ON
+108°
-108°
22°/s
0
7 sec
B_i
+35°
-35°
-108°
+108°
22°/s
B_ii
Weber contrast
470 nm
grayscale
OFF
ON
C_i
LC15 dendrites
1 ΔF/F0
C_ii
saline flies
100 μM 5-HT flies
C_iii
effect strength
0
7 sec
H_i
LC15 axon terminals
1 ΔF/F0
H_ii
1 ΔF/F0
H_iii
+1 ΔF/F0
-1 ΔF/F0
0
7 sec
D
Mean F
p = 0.57
I
Mean F
p = 0.88
E
Max ΔF/F0
p = 0.54 p = 0.66 p = 0.30 p = 0.71 p = 0.83 p = 0.36 p = 0.28 p = 0.80
J
Max ΔF/F0
p = 0.87 p = 0.84 p = 0.43 p = 0.13 p = 0.58 p = 0.25 p = 0.95 p = 0.95
F
Integrated Ca2+
p = 0.67 p = 0.47 p = 0.40 p = 0.71 p = 0.70 p = 0.10 p = 0.19 p = 0.84
K
Integrated Ca2+
p = 0.94 p = 0.55 p = 0.13 p = 0.26 p = 0.73 p = 0.39 p = 0.67 p = 0.80
G
-1.0 p = 0.51
-0.8 p = 0.42
-0.6 p = 0.26
-0.3 p = 0.93
0.3 p = 0.77
0.6 p = 0.28
0.8 p = 0.45
1.0 p = 0.41
Time (sec)
L
-1.0 p = 0.06
-0.8 p = 0.44
-0.6 p = 0.20
-0.3 p = 0.50
0.3 p = 0.06
0.6 p = 0.93
0.8 p = 0.41
1.0 p = 0.92
Time (sec)

Figure 3. Dendritic and axonal LC15 responses show no effect of bath-applied 5-HT on luminance polarity

(A) Motion of the visual feature over time (bottom). The bar of varying luminance levels moved at a constant velocity of 22 °/sec across the right side of the LED display.
(Bi) LED display schematic illustrating the 8.8° x 70° vertical bar stimulus presentation.
(Bii) Weber contrast profile of the eight tested luminance levels.
(Ci) Population mean GCaMP6f signal from the LC15 dendrites (± SEM shading) before (gray) and after 100 μM 5-HT (cyan). The horizontal scale bar (black) represents 1 second.
(Cii) $\Delta F/F_0$ response raster plots displaying mean animal responses before (top) and after 100 μM 5-HT (bottom) (N = 10). Flies 1-10 (rows) are sorted the same in the pre-5-HT (top) and post-5-HT (bottom) condition rasters.
(Ciii) Mean change in effect size rasters of LC15 dendritic GCaMP6f responses for each animal in the saline and 5-HT experimental groups. Animals (row) are sorted by increasing effect size strength.
(D) Pairwise comparison of mean fluorescent intensity in the LC15 dendrites before (gray) and after 100 μM 5-HT (cyan). Horizontal red lines correspond to the population means. Two-tailed paired t-test, N = 10.
(E) Pairwise comparison of maximum $\Delta F/F_0$ responses in the LC15 dendrites before (gray) and after 100 μM 5-HT (cyan). Two-tailed paired t-test, N = 10.
(F) Pairwise comparison of integrated Ca^{2+} responses in the LC15 dendrites before (gray) and after 100 μM 5-HT (cyan). Two-tailed paired t-test, N = 10.
(G) Pairwise comparison of time to half-max (sec) for LC15 dendrite responses before (gray) and after 100 μM 5-HT (cyan). Two-tailed paired t-test, N = 10.
(Hi) Population mean GCaMP6f signal from the LC15 glomerulus (± SEM shading) before (gray) and after 100 μM 5-HT (cyan). The vertical scale bar (black) represents 1 $\Delta F/F_0$. The horizontal scale bar (black) represents 1 second.
(Hii) $\Delta F/F_0$ response raster plots displaying mean animal responses before (top) and after 100 μM 5-HT (bottom) (N = 22). Flies 1-22 (rows) are sorted the same in the pre-5-HT (top) and post-5-HT (bottom) condition rasters.
(Hiii) Mean change in effect size rasters of LC15 glomerular GCaMP6f responses for each animal in the saline to 5-HT experimental groups. Animals (row) are sorted by increasing effect size strength.
(I) Pairwise comparison of mean fluorescent intensity in the LC15 glomerulus before (gray) and after 100 μM 5-HT (cyan). Horizontal red lines correspond to the population means. Two-tailed paired t-test, N = 22.
(J) Pairwise comparison of maximum $\Delta F/F_0$ responses in the LC15 glomerulus before (gray) and after 100 μM 5-HT (cyan). Two-tailed paired t-test, N = 22.
(K) Pairwise comparison of integrated Ca^{2+} responses in the LC15 glomerulus before (gray) and after 100 μM 5-HT (cyan). Two-tailed paired t-test, N = 22.
(L) Pairwise comparison of time to half-max (sec) for LC15 glomerulus responses before (gray) and after 100 μM 5-HT (cyan). Two-tailed paired t-test, N = 22.

It is worth noting that mean peak $\Delta F/F_0$ values are larger for the solid bar than for the motion defined bar (compare Figure 2Aii second column with Figure 3Ci first column). This indicates that the dendritic GCaMP responses to the motion-defined bar in Figure 2 are not saturated or 'clipped'. There is physiological 'headroom' in LC15 dendrites for 5-HT potentiation to have been manifested, but it is not. Taken together with the absence of contrast modulation suggests to us that 5-HT is unlikely to be acting upon ON or OFF presynaptic inputs to LC15 dendrites, but rather on the presynaptic terminals of LC15 itself in the glomerulus.

5-HT normalizes velocity responses by LC15

The strong dendritic response to a dark bar (Figure 3C) motivated us to use this low frequency luminance-defined stimulus, rather than the high frequency motion-defined bar, to test whether 5-HT modulates LC15 responses to varying object velocity. We tested an 8.8° x 70° OFF bar moving at 22, 44, 66, 88, 110, 132°/s (Figure 4Ai) in randomized order. Results from presynaptic glomerulus recordings are shown in Figure 4 and the corresponding results from postsynaptic dendrites can be found in Figure S1. LC15 responded best to the slowest-velocity OFF bar, and

was attenuated with increased bar speed (Figure 4Aii). Speed attenuation was not observed in the dendrites (Figure S1), rather responses were essentially normalized across velocity, confirming previous findings (Städele et al. 2020). Remarkably, in the glomerulus, 5-HT delivery was accompanied by potentiated responses to higher bar velocities (Figure 4Aii,Aiii) across animals in the experimental cohort (Figure 4Aiv,Av).

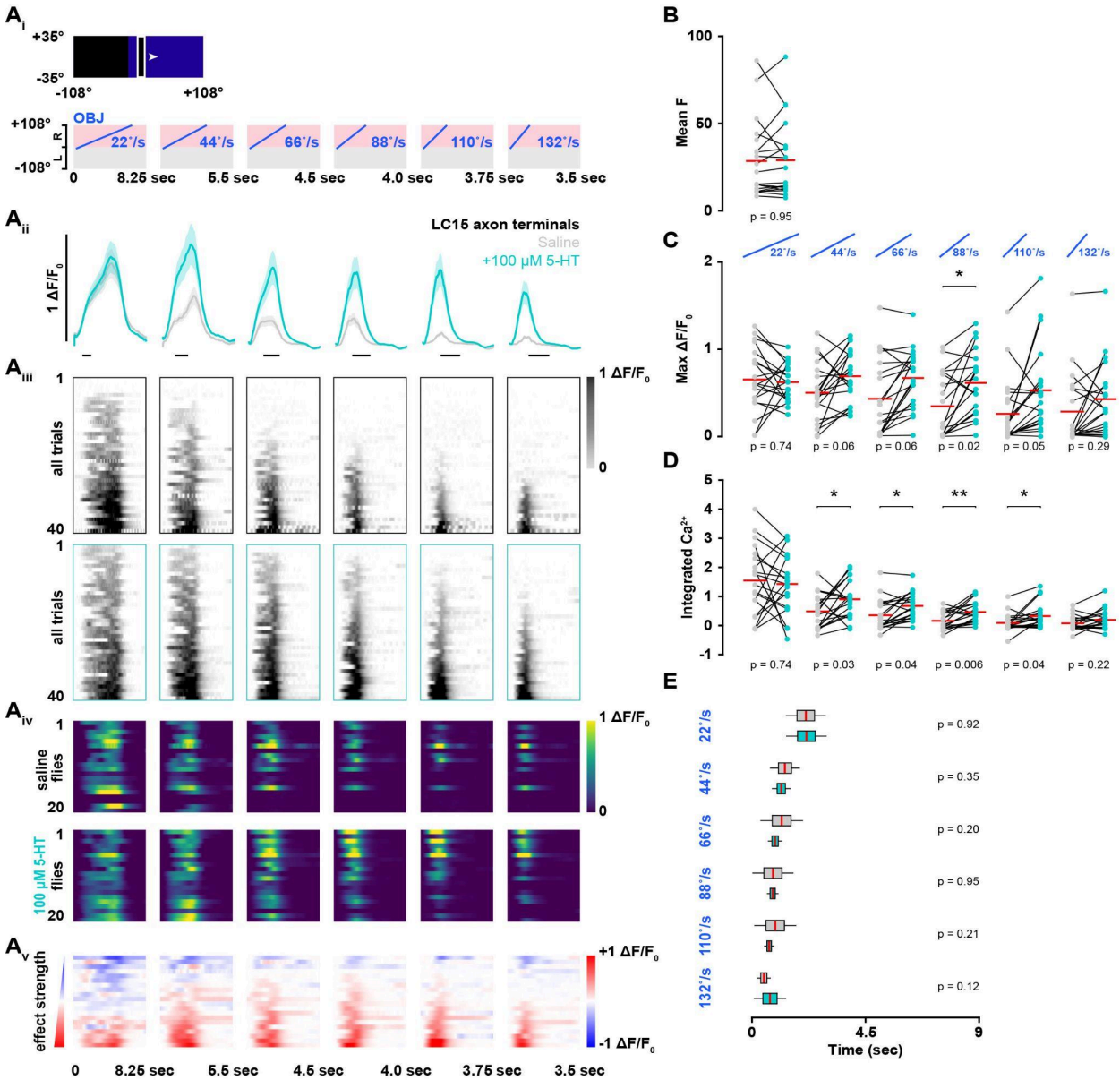

Figure 4. LC15 glomerular responses to OFF bar velocity are selectively potentiated by 5-HT

(Ai) Schematic illustrating the 8.8° x 70° vertical bar presented on the LED display (top) and the motion of the translating feature over time (bottom). The OFF bar moved at six different velocities (22, 44, 66, 88, 110, and 132 °/sec) across the right side of the LED display.

(Aii) Population mean GCaMP6f signal from the LC15 glomerulus (± SEM shading) before (gray) and after 100 µM 5-HT (cyan). The horizontal scale bar (black) represents 1 second.

(Aiii) $\Delta F/F_0$ response raster plots displaying individual trial responses before and after 100 μM 5-HT (cyan). Two repeats of each stimulus were shown to each animal (N = 20, n = 40). The trial responses are sorted by increasing peak $\Delta F/F_0$ response.
(Aiv) $\Delta F/F_0$ response raster plots displaying mean animal responses before (top) and after 100 μM 5-HT (bottom) (N = 20). Flies 1-20 (rows) are sorted the same in the pre-5-HT (top) and post-5-HT (bottom) condition rasters.
(Av) Mean change in effect size rasters of LC15 glomerular GCaMP6f responses for each animal in the saline to 5-HT experimental group. Animals (row) are sorted by increasing effect size strength.
(B) Pairwise comparison of mean fluorescent intensity in the LC15 glomerulus before (gray) and after 100 μM 5-HT (cyan). Two-tailed paired t-test, N = 20.
(C) Pairwise comparison of maximum $\Delta F/F_0$ responses in the LC15 glomerulus before (gray) and after 100 μM 5-HT (cyan). Two-tailed paired t-test, N = 20.
(D) Pairwise comparison of integrated Ca^{2+} responses in the LC15 glomerulus before (gray) and after 100 μM 5-HT (cyan). Two-tailed paired t-test, N = 20.
(E) Pairwise comparison of time to half-max (sec) for LC15 glomerulus responses before (gray) and after 100 μM 5-HT (cyan). Two-tailed paired t-test, N = 20.

5-HT perfusion was not accompanied by a change in baseline GCaMP fluorescence, suggesting that velocity normalization was not mediated by tonic Ca^{2+} accumulation (Figure 4B). The mean peak GCaMP response for the slowest 22°/s bar was unchanged, but the fastest velocities caused a statistically significant increase in peak $\Delta F/F_0$ at 88°/s (Figure 4C). The responses to the other high velocity bars were likewise increased however not individually significant (Figure 4C). The time-integrated Ca^{2+} responses showed that 5-HT significantly increased visually evoked Ca^{2+} accumulation for bars presented at 44, 66, 88, and 110°/s (Figure 4D). 5-HT did not significantly affect the onset delay of the visual response (Figure 4E). None of these significant changes were observed in the mean lobula dendrites (Figure S1B,C). As with figure-ground discrimination (Figure 1), velocity normalization localized to the axon terminals implicates neuromodulation targets within circuits of central brain glomeruli, rather than within retinotopic inputs from the optic lobe.

A similar bar sensitive feature detector, LC12, is not modulated by serotonin

We next sought to test whether 5-HT has similar effects on other LC types, and examined another bar motion sensitive detector, LC12 (Figure 5A). As with LC15, we did not observe any change in baseline fluorescence after 5-HT application in LC12; neither did we observe any modulation of visual responses. Figure 5B shows the results from the motion-defined bar over WF background experiment used in Figures 1 and 2. We observed low amplitude responses in the LC12 glomerulus to the motion-defined bar, but no potentiation from 5-HT application (Figure 5B). We measured a subtle yet statistically significant *reduction* in the mean $\Delta F/F_0$ response to the third stimulus condition, a static bar defined by the WF, after 5-HT bath application (Figure 5Ci). The integrated Ca^{2+} response for this stimulus sequence was significantly reduced as well (Figure 5Cii). We tested bars of varying luminance levels (Figure 5D), or velocities (Figure 5E), but did not observe any changes after 5-HT application (Figure S2). Taken together, our recordings from LC12 and LC15 indicate that serotonergic modulation of visual responses is cell type specific even within the family of structurally similar feature detectors and modulation acts selectively in the presynaptic compartment.

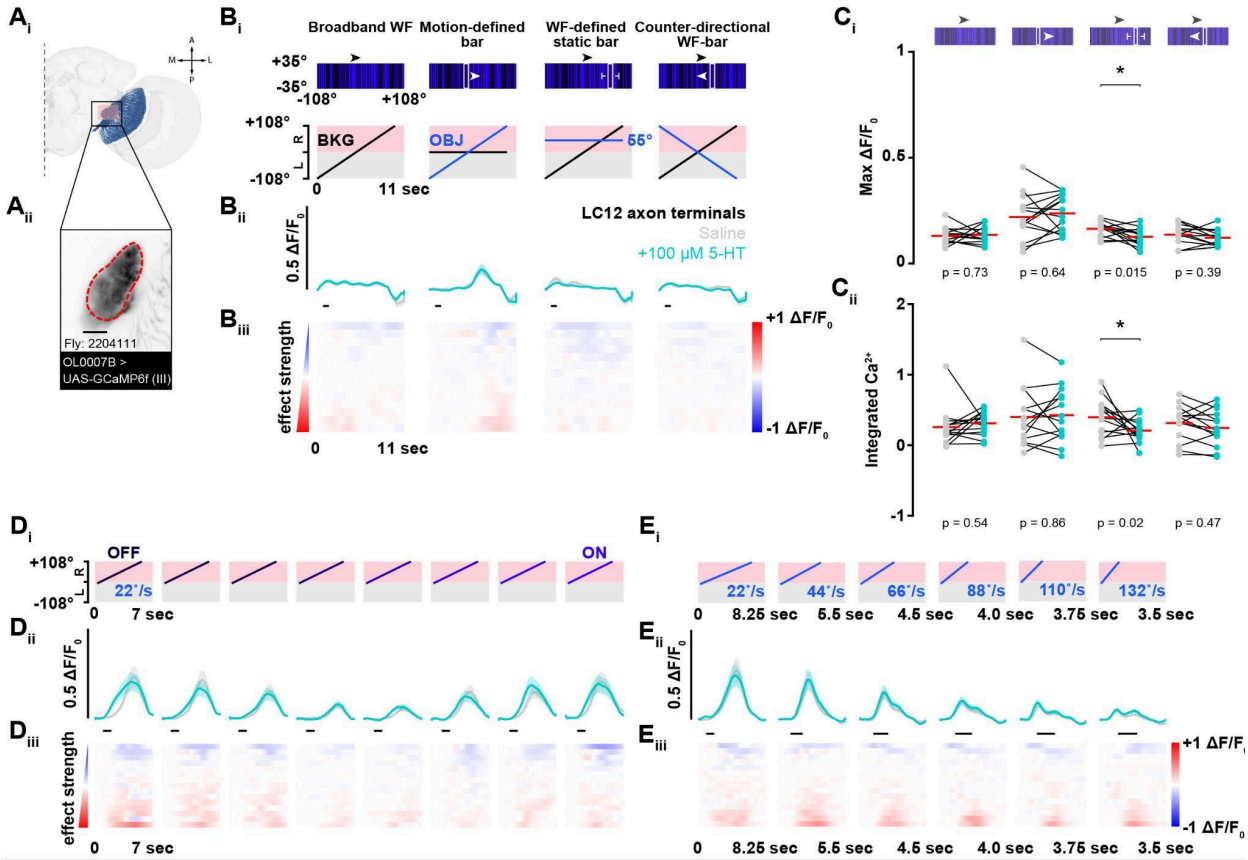

Figure 5. The LC12 glomerulus does not show potentiation to translating vertical bars after 5-HT bath perfusion

(Ai) FlyWire connectome reconstruction of LC12 cells (blue) in the right hemisphere. The pink box represents the imaging site of the LC12 glomerulus. The LC12 dendritic projections receive signals in the lobula and send that information downstream to the glomerulus in the VLP.

(Aii) Two-photon fluorescent intensity image showing the glomerulus, or axonal bundle of LC12 cells. The red dotted line defines the region of interest. Scale bar, 25 μm.

(Bi) Schematic showing the visual stimulus presented on the LED display (top) and the motion of the visual feature elements over time (bottom). The second column displays the LC12 glomerular response to a motion-defined equiluminant vertical bar over a stationary broadband background before (gray) and after bath perfusion of 100 μM 5-HT (cyan) in saline.

(Bii) Population mean GCaMP6f signal from the LC12 glomerulus (± SEM shading) before (gray) and after 100 μM 5-HT (cyan).

(Biii) Mean change in effect size rasters of LC12 glomerular GCaMP6f responses for each animal in the saline and 5-HT experimental groups. Animals (row) are sorted by increasing effect size strength.

(Ci) Pairwise comparison of maximum $\Delta F/F_0$ responses in the LC12 glomerulus before (gray) and after 100 μM 5-HT (cyan). Two-tailed paired t-test, N = 14.

(Cii) Pairwise comparison of integrated Ca^{2+} responses in the LC12 glomerulus before (gray) and after 100 μM 5-HT (cyan). Two-tailed paired t-test, N = 14.

(Di) Motion of the visual feature over time. The bar of varying luminance levels moved at a constant velocity of 22 °/sec across the right side of the LED display.

(Dii) Population mean GCaMP6f signal from the LC12 glomerulus (±SEM shading) before (gray) and after 100 μM 5-HT (cyan).

(Diii) Mean change in effect size rasters of LC12 glomerular GCaMP6f responses for each animal from the saline to 5-HT condition.

(Ei) The motion of the translating feature over time. The OFF bar moved at six different velocities (22, 44, 66, 88, 110, and 132 °/sec) across the right side of the LED display.
(Eii) Population mean GCaMP6f signal from the LC12 glomerulus (±SEM shading) before (gray) and after 100 μM 5-HT (cyan).
(Eiii) Mean change in effect size rasters of LC12 glomerular GCaMP6f responses for each animal in the saline and 5-HT experimental group.

Connectomics reveal multiple inhibitory circuit motifs with putative serotonergic LC15 interactions

We used the FlyWire EM reconstruction connectome database to examine the chemical synaptic partners of LC15 (Dorkenwald et al. 2024). This resource labels all of the synaptic partners in the brain but, unfortunately, cannot identify extrasynaptic paracrine partners involved in volumetric hormonal neuromodulation. The connectome does however provide us with a wealth of information about the participating neurons including the neural architecture of the two feature-processing VPNs studied here. First, we examined the connectome for any shared upstream inputs to both LC12 and LC15, starting with the lamina monopolar neurons L1-L5. We also identified the downstream partners of these two LCs for potential serotonergic intersections.

The major inputs by synaptic count to LC15 include TmY4, Li27, TmY9q⊥, TmY9q, Li31, PVLP101b, CB0346, Tm25, PVLP103, and LmA2. TmY4, TmY9q⊥, and TmY9q are three horizontally-oriented neurons predicted to prefer OFF objects along their axis of orientation. Other strong LC15 disynaptic pathways include T3, a small-object detector, and other object-detecting cells, Tm25 and Tm21 (Seung 2024). This report also showed that three populations of glutamatergic neurons (Dm3q, Dm3p, Dm3v) play a critical role in filtering OFF activated signals supplied to LC15. TmY4, TmY9q⊥, TmY9q, Li30, and Tm25 are cholinergic. PVLP103, CB0346, PVLP101b and CB0140 are GABAergic. Li27 is glutamatergic (Table 1). The major outputs from LC15 by synaptic count are PVLP121, CB0381, CB2049, PLP115_b, CB0346, PVLP028, PVLP118, LT61b, PVLP151, and PVLP018 (Table 2).

The major inputs to LC12 are Tm3, Tm4, PVLP097, T2, TmY3, Li17, TmY11, cL21, T3, and Tm2. The connectome shows that L2 synapses onto Dm17 which connects to TmY3. L2 also synapses onto Tm4 (implicated in the OFF motion pathway), which has connections to Li31, a GABAergic inhibitory neuron that crosses the midline of the brain and connects to the LC15 glomerulus on the contralateral hemisphere. Tm3, Tm4, T2, TmY3, TmY11, T3, and Tm2 are cholinergic. PVLP097, Li17, and cL21 are GABAergic (Table 3). The major outputs from LC12 by synaptic count are PVLP097, PVLP025, PVLP013, PVLP037, CB0813, CB1340, cL21, PVLP120, PVLP100, and AVLP152 (Table 4). These results indicate that LC12 and LC15 share no major zero hop presynaptic inputs, and only a single one-hop input from L5. L5 itself may express 5-HT7 but this has yet to be confirmed (Sampson et al. 2020).

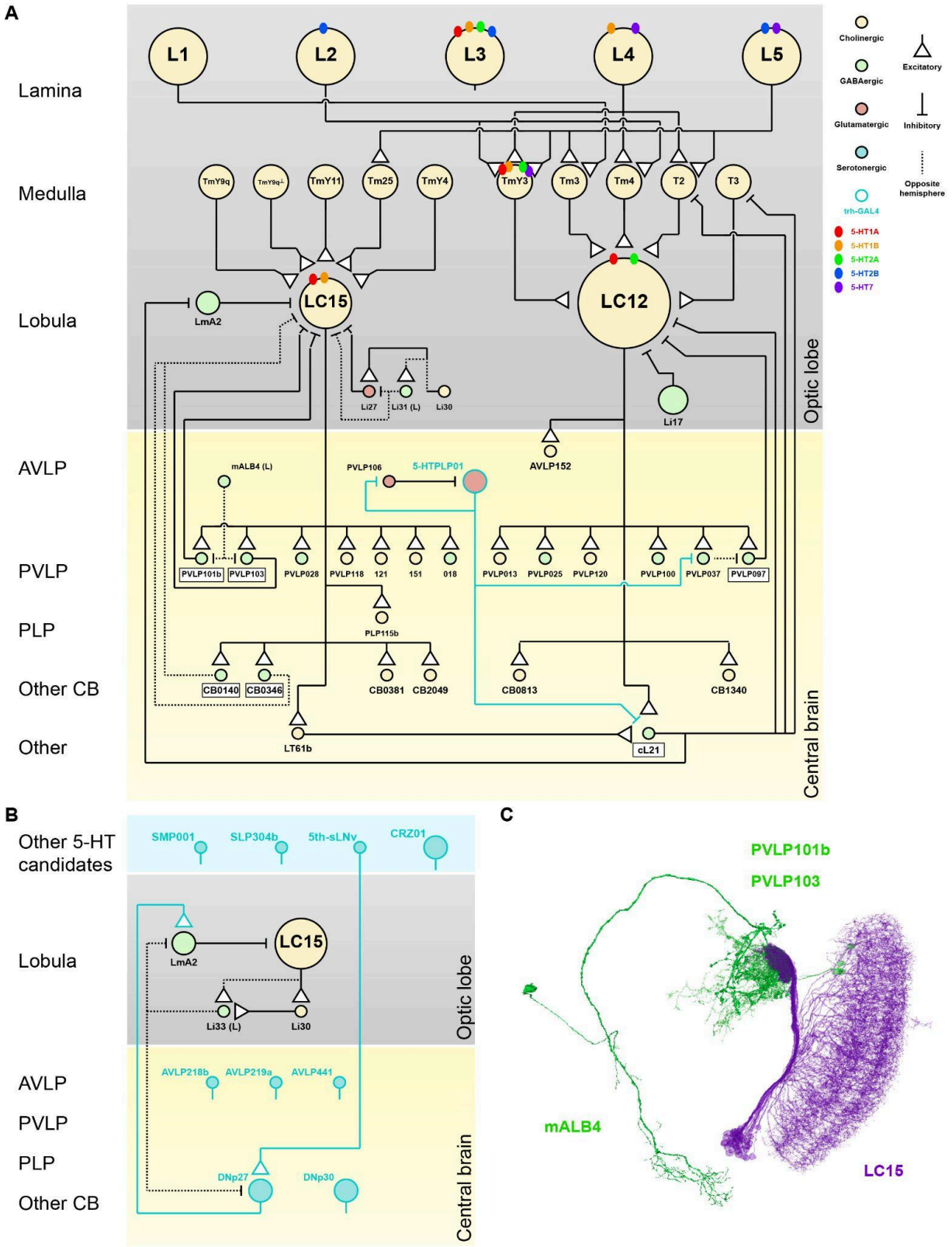
A
Lamina
Medulla
Lobula
AVLP
PVLP
PLP
Other CB
Other
L1
L2
L3
L4
L5
TmY9q
TmY9q⊥
TmY11
Tm25
TmY4
TmY3
Tm3
Tm4
T2
T3
LC15
LC12
LmA2
Li27
Li31 (L)
Li30
Li17
Optic lobe
mALB4 (L)
PVLP106
5-HTPLP01
AVLP152
PVLP101b
PVLP103
PVLP028
PVLP118
121
151
018
PVLP013
PVLP025
PVLP120
PVLP100
PVLP037
PVLP097
PLP115b
CB0140
CB0346
CB0381
CB2049
CB0813
CB1340
LT61b
cL21
Central brain
Cholinergic
GABAergic
Glutamatergic
Serotonergic
trh-GAL4
5-HT1A
5-HT1B
5-HT2A
5-HT2B
5-HT7
Excitatory
Inhibitory
Opposite hemisphere
B
Other 5-HT candidates
SMP001
SLP304b
5th-sLNv
CRZ01
Lobula
LmA2
LC15
Li33 (L)
Li30
Optic lobe
AVLP
PVLP
PLP
Other CB
AVLP218b
AVLP219a
AVLP441
DNp27
DNp30
Central brain
C
PVLP101b
PVLP103
mALB4
LC15

Figure 6. Connectomics highlights specific circuit motifs and candidate sites for 5-HT neuromodulation

(A) Wiring diagram of LC15 and LC12 illustrating the connections between the major presynaptic and postsynaptic partners and the synaptic connections to 5-HTPLP (Dorkenwald et al. 2024). Cells are colored by neurotransmitter type and are stratified by neuropil. The colored dots detail the 5-HTR expression where available. Bordered cell names refer to neurons that both send and receive synapses from LC15 or LC12. The 5HTPLP01 is labelled by trh-GAL4 (cyan) but uses glutamate as its neurotransmitter so the connections to downstream partners are shown as inhibitory. 5-HTPLP01 makes reciprocal connections to another glutamatergic neuron, PVLP106. 5-HTPLP01 makes the largest number of synapses onto cL21 (703, 6%) but otherwise does not make connections to the members of the LC15 pathway. cL21 is a pair of centrifugal GABAergic cells that have input synapses in the PVLP and outputs in the lobula. Both PVLP106 and cL21 receive most of their input synapses from LC17 (3,743, 54% and 4,560, 25%). 5-HTPLP01 does synapse onto a downstream target of LC12, a GABAergic cell class called PVLP037. PVLP037 has 4 cells per hemisphere and makes 684 inhibitory synapses onto PVLP097, a recursive partner of LC12. 5-HTPLP01 sends and receives most of its connections from AVLP interneurons.

(B) The neurons of the right hemisphere that have output synapses in the PVLP and use 5-HT as a neurotransmitter (cyan). Direct connections to the LC15 VPN network are also shown. The only serotonergic cell that synapses onto members of the LC15 pathway is DNp27. DNp27 is a large bilateral descending neuron that innervates the right SMP, PLP, PVLP and AVLP. Output synapses are observed in the central brain and in the lobula but presumably most outputs are located in the VNC (tectulum, lower tectulum, and abdominal segment, see (Namiki et al. 2018)). In the lobula, DNp27 makes synapses onto a population of 17 lobula-medulla amacrine cells, LmA2. The LmA2 cells make up a patchwork tiling the visual field and the LmA2 cells make 583 synapses onto LC15 in the lobula.

(C) Morphology of the mALB4-PVLP101b-PVLP103-LC15 circuit element. LC15 (purple) and the GABAergic partners (green) that interact at the LC15 glomerulus. mALB4 is a GABAergic neuron that has input synapses in the PVLP and the SEZ. The output synapses are solely located in the PVLP, where it connects to PVLP101b and PVLP103. PVLP101b contains two GABAergic cells that have reciprocal (input and output) synapses with LC15. PVLP103 similarly contains two GABAergic cells that receive 341 synapses from LC15 and makes 593 synapses back onto LC15.

Figure 6A displays a connectivity diagram between the top ten pre- and postsynaptic partners to LC15 and LC12, stratified by neuropil from the optic lobe into the central brain. The top ten pre- and postsynaptic partners to LC15 and LC12 are also shown and colored by their putative neurotransmitter type. It should be noted that this is a non-exhaustive list meant to highlight similarities or differences in the chemical synaptic wiring between these two bar-sensitive object detectors. We also queried the database for synapses between serotonergic 5-HTPLP01 and our LCs of interest or their immediate partners, but we did not identify any. Interestingly, 5-HTPLP01 may co-release 5-HT volumetrically and glutamate synaptically (see Nässel 2009; Nässel and Homberg 2006; Schäfer et al. 2002). 5-HTPLP01 does connect indirectly to LC15 through a centrifugal GABAergic interneuron, cL21, which provides feedback inhibition to LC12 and synapses onto another set of GABAergic neurons, LmA2. LmA2 connects to LC15 dendrites at the lobula (Figure 6A, Figure S4B). Tables 5 and 6 list the top ten pre- and postsynaptic partners for 5-HTPLP01. The strongest synaptic input to 5-HTPLP01 comes from ALVP169, cholinergic cells that make reciprocal synapses onto 5-HTPLP01 from the AVLP, but 5-HTPLP01 also receives GABAergic input from CB0534 and AVLP081, and glutamatergic input from PVLP106 (Figure S3A,S3C).

I. Peripheral optic lobe

We queried the FlyWire connectome database to identify any serotonergic neurons (i.e. neurons that use 5-HT as a neurotransmitter) that interact with LC15. We observed that only one, the expansive serotonergic descending neuron, DNp27, makes synaptic connections onto GABAergic LmA2 neurons in the lobula, which in turn synapse onto LC15 (Figure 6B) (see Namiki et al. 2018). DNp27 receives inputs from another serotonergic neuron, 5th-s-LNv which is a member of the evening oscillator in the circadian clock circuitry and required for a bimodal sleep-activity rhythm (Hevers and Hardie 1995; Nässel 2018; Shafer et al. 2022; Yuan et al. 2005). Figure 6B displays the connectivity between all serotonergic neurons with synaptic output to the numerically top ten pre- and postsynaptic partners to LC15 and LC12, stratified by neuropil from the optic lobe into the central brain. When the 5th-s-LNv is activated, this could enhance responses from DNp27, to increase the GABAergic tone in the lobula through the LmA2 amacrine cells at a particular time in the circadian rhythm.

This analysis uncovered another lobula circuit element where lateral inhibitory neurons in the lobula interact directly, or indirectly through the glutamatergic lateral neurons, Li27. There are two Li27 neurons per hemisphere that form numerous synapses onto the dendrites of LC15 (1,670 synapses to all LC15 cells, 24% of all inputs). Li27 receives input from TmY4, TmY9q⊥, and TmY9q as well as a GABAergic interneuron, Li31. Li31 receives cholinergic inputs from Tm4 and Tm3 but also from a lateral neuron, Li30 (Figure S4A) before synapsing onto Li27 and LC15. Li30 is a cholinergic cell upstream of Li31 which receives most of its synapses from Y3. These three cells are positioned to act as a gain control mechanism upon LC15 in the lobula, independent of the two glomerular motifs downstream. The glutamatergic Li27 cells may provide shunting inhibition of LC15 to filter out noise from object stimuli.

II. Central brain

Two glomerulus-specific circuit motifs were also uncovered: 1) contralateral suppression and 2) gain control through release from inhibition. The wiring diagram suggests that the neural architecture exists to provide contralateral GABAergic suppression in LC15. Downstream partners of LC15, CB0140 and CB0346 are GABAergic cells that innervate the LC15 glomerulus and synapse onto the other LC15 glomerulus (Figure S5B). This axo-axonal suppression appears similar to what has previously been reported in another different LC, LC6 (Morimoto et al. 2020).

Our connectivity analysis also shows that LC15 makes connections to PVLP101b and PVLP103 in the OG. These GABAergic lateral inhibitory neurons also make reciprocal synapses back onto LC15 and presumably provide the majority of the inhibitory tone at the LC15 glomerulus through feedback inhibition. PVLP101b and PVLP103 both share an upstream partner, mALB4, a GABAergic neuron from the left hemisphere that synapses at the LC15 glomerulus but does not make direct connections to the LC15 cells themselves. The dendritic arbor of the mALB4 neuron also innervates the subesophageal zone, SEZ (Figure 6C) (Figure S5A). LC12 makes reciprocal synapses with a population of lateral inhibitory neurons, PVLP097. There are 7 GABAergic PVLP097 cells per hemisphere that make reciprocal synapses with LC12. PVLP097

is LC12's highest output partner (15,920, 28%), and LC12 is PVLP097's highest output partner (2,403, 25%). PVLP037 constitutes 4 GABAergic neurons upstream of PVLP097 that cross hemispheres (794, 4%). 5-HTPLP makes glutamatergic synapses onto PVLP037 (98, 1%) (Figure S6).

Discussion

Receptor expression does not predict neuromodulation of visual responses

As in vertebrates, multiple serotonin receptor (5-HTR) subtypes have been identified in *Drosophila* that initiate both excitatory and inhibitory GPCR-mediated functions (Ciranna 2006; Gasque et al. 2013; Saudou et al. 1992; Witz et al. 1990). Five subtype receptors coupled to identified GPCRs have been identified in *Drosophila* (5-HT1A, 5-HT1B, 5-HT2A, 5-HT2B, and 5-HT7) that cause specific metabolic cascades through second messenger systems. Two of these receptors inhibit cAMP synthesis (5-HT1A, 5-HT1B), decreasing intracellular Ca^{2+} levels. The other three either promote cAMP production through activation of adenylate cyclases (5-HT7), or mediate hydrolysis of inositol phosphates (5-HT2A, 5-HT2B) leading to increased intracellular Ca^{2+} levels (Blenau and Thamm 2011; Sizemore and Dacks 2016). 5-HTR expression was distinct for each receptor subtype in the adult brain neuropils including the mushroom bodies (MB), central complex (CX), optic lobes (OL) and antennal lobes (AL) (Mallick et al. 2024). The 5-HTR expression profile is different between LC12 and LC15; LC15 displays high levels of 5-HT1A and 5-HT1B (Bonanno et al. 2024); YZ Kurmangaliyev, personal communication). Both 5-HT1A and 5-HT1B are coupled to the $G_{i/o}$ GPCR which reduces cytosolic cAMP through the inhibition of adenylate cyclase (AC) activity. Immunohistochemistry analysis revealed that LC12 shows high levels of 5-HT1A and 5-HT2A in the presynaptic axon terminals of the glomerulus but not the postsynaptic dendrites in the lobula. 5-HT2A receptors are coupled to the GPCR $G_{q/11}$, and activation leads to the hydrolysis of inositol phosphates and a subsequent intracellular Ca^{2+} increase. Sparse synaptic labeling of 5-HT suggests that the LC glomeruli in the VLP receive most of their serotonergic modulation via volumetric release of the neuromodulator (Bonanno et al. 2024).

A class of columnar neurons upstream of the LCs, lamina monopolar L2, show 5-HT sensitivity. L2 cells express 5-HT1A and 5-HT2B, and upon administration of exogenous 5-HT, showed a gradual increase in basal Ca^{2+} fluorescence in medulla layer M2 over the 6-minute time frame. This effect was dramatically reduced in 5-HT2B$^{-/-}$ mutant flies. 5-HT2B, like 5-HT2A, are coupled to $G_{q/11}$, suggesting that 5-HT activation of 5-HT2B on L2 neurons may enhance the response to OFF objects (i.e. objects darker than the background). This report suggests that the 5-HT2B receptor is necessary for serotonergic potentiation of L2 Ca^{2+} responses observed in the lamina (Sampson et al. 2020). L2 is an upstream input for LC12 but not LC15 and we show that these two VPN populations do not share any common partners directly upstream (Figure 6A). It is possible that a feed-forward modulatory effect of 5-HT on L2 potentiates OFF responses in downstream partners, like LC12. Lastly, neither LC12 or LC15 express 5-HT7, but recent work has shown that 5-HT7-expressing GABAergic LNs in the antennal lobe mediate subtractive gain control in the PNs of the CO_2-sensitive V glomerulus (Mallick et al. 2024). In these inhibitory cells, 5-HT7 activates the Gs protein, which stimulates AC, increasing intracellular cAMP (Gajardo et al. 2023; Sizemore et al. 2020; Vleugels et al. 2014).

Here, we show that 5-HT modulation is highly selective within the LC feature detection pathway. The effects of 5-HT application are (i) stimulus-specific, enhancing responses to bar motion but not ground motion (Figure 1); (ii) they are anatomically compartmentalized, appearing in the axon terminals but not the dendrites (Figure 2); (iii) selective for visual stimulus parameters, as 5-HT application has no influence over luminance tuning (Figure 3), yet boosts responses to normalize bar velocity (Figure 4); finally, (iv) the effects of 5-HT application are cell-type specific, modulating LC15 but not LC12 (Figure 5).

These results are unexpected given that LC15 purportedly expresses 5-HTRs that inhibit adenylate cyclase (Blenau and Thamm 2011); YZ Kurmangaliyev, *personal communication*). By contrast, we expected to observe a potentiation effect in LC12. What is the role of excitatory 5-HT2A receptors on LC12 cells if not for modulating visual responses or to increase basal Ca^{2+}? 5-HT is involved in a multitude of physiological mechanisms and behavioral phenotypes. 5-HTR expression has been shown to be involved in 'higher order' biological functions such as the entrainment of circadian rhythm, aggression, and courtship circuitry, or cell metabolic functions where 5-HT may play a role (Dierick and Greenspan 2007; Pooryasin and Fiala 2015; Yuan et al. 2005).

Serotonin bath application, and presumably volumetric release in the VLP, reveals a coordinated increase in the feature-detecting parameter space

Bath application of any neuromodulator is experimentally convenient and is the only way to demonstrate the specificity of the signal rather than indirect action via another neuromodulator. Under normal conditions, endogenous 5-HT likely fills the ventrolateral protocerebrum (VLP) *via* volumetric release through 5-HTPLP01 to cause non-cell-autonomous neuromodulatory effects on lobula columnar (LCs) cells (Aimon et al. 2023; Alekseyenko and Kravitz 2014; Bonanno et al. 2024). This serotonergic activity in the VLP is likely to be extra-synaptic since 5-HTPLP is glutamatergic (Figure 6A). Our results are therefore notable in that the effects of bath application come on quickly, are object-stimulus-specific, cell-type-specific, and subcellular domain-specific (Figure 1-5). Indeed, there was no stimulus parameter that was shared across any response dimension we could find. Our results also suggest that neuromodulatory changes in VPN responses are not simply controlled through activation of volumetric peptidergic neurons but through iLN activation that leads to specific downstream release from feedback inhibition. Previous behavioral experiments performing optogenetic targeting of trh-gal4 showed that a rigidly-tethered fruit fly tracks a bar significantly better during LED stimulation but had no effect on the small-object response (Cheng et al. 2019). These activation experiments (trh-gal4 > UAS-CsChrimson) are unlikely to fully capture the effect of state-dependent changes in sensorimotor transduction unless the inhibitory partners are also controlled. There is no way of knowing from these results if 5-HT is specifically causing this phenotype; it could result from downstream partners of serotonergic neurons instead of non-synaptic hormonal release (Figure 6B). To best mimic the neuromodulatory conditions for the LC15 glomerulus, optogenetic targeting of trh-gal4 serotonin-releasing neurons was insufficient to be used alone. The most parsimonious explanation is that 5-HT is acting extrasynaptically on a subset of

glomerulus-specific inhibitory partners to enhance select visual responses in LC15 (Figure 6). The 5-HTR profiles of these lateral inputs are as yet unknown.

Identifying feedforward and feedback potentiation of feature detection

In the VLP, circuit-level potentiation may include increasing the gain of opposing cell classes (e.g. cholinergic and GABAergic cells) to allow for changes in the visual feature parameter space or SNR. Bath applications of 5-HT in brain explants result in increased Ca^{2+} activity in both GABAergic 5-HT1A receptor-expressing neurons, as well as cholinergic short neuropeptide F receptor and 5-HT1A receptor-expressing neurons (Alekseyenko et al. 2019). 5-HT may change the activity or responsiveness of these inhibitory cells, thereby affecting the GABAergic tone over LC15. If not through the direct effects of 5-HT onto the LC15 cells themselves, the potentiation of LC15 by 5-HT must be caused in a non-autonomous manner by a change in another element of the visual feature detection pathway. The two most likely non-autonomous ways for this potentiation to take place would be through 1) feedforward excitation, or 2) release from feedback inhibition. Feedforward excitation would involve serotonergic potentiation of excitatory inputs and/or decrease in inhibitory inputs upstream of LC15 in the optic lobe to increase the 'gain'. Release from feedback inhibition would be characterized by top-down inhibition of GABA-releasing inhibitory cells intrinsic to the LC15 glomerulus.

If potentiation in LC15 were predominantly controlled by feedforward excitation, we reason that 5-HT would act upon presynaptic inputs to LC15 expressing excitatory 5-HTRs. Here, 5-HT would increase cholinergic activity upstream of LC15, presumably through TmY cells. Inhibitory 5-HTRs might also be located on Dm cells which synapse onto LC15 in the lobula. The potentiated responses would be relayed from the lobula to the glomerulus. We did not observe significant potentiation of LC15 responses in the lobula to any stimulus after 5-HT. Our dendrite recordings also support previous research showing a lack of velocity-tuned responses in the dendrites (Klapoetke et al. 2022; Städele et al. 2020).

If potentiation in LC15 were caused by release from feedback inhibition, this would require evidence of inhibitory cells that send and receive synapses to LC15. These partners must also be contained to the cellular subdomain of the OG, and that the OG are under some degree of active inhibitory control. 5-HT would disinhibit specific glomeruli in two ways (i) 5-HT inhibits GABAergic partners at the LC15 glomerulus (via 5-HT1A, or 5-HT1B), or (ii) 5-HT excites inhibitory GABAergic cells that themselves synapse onto inhibitory partners of LC15 (5-HT2A, 5-HT2B, or 5-HT7). Our experimental results suggest that in LC15, the individual retinotopically-arranged dendrites in the lobula are pooled together at the OG and that 5-HT has direct effects on the excitability of the presynaptic partners in the VLP. Through cotransmission, 5-HTPLP01 may inhibit downstream synaptic partners with glutamate signaling, and through hormonal release of 5-HT, activate others in the PVLP. 5-HT release potentiates responses in the LC15 glomerulus to select context-specific features while strengthening the filter through active inhibition. This increase in sensitivity (LmA2 release from inhibition via cL21, Figure 6B) is temporally linked with the release of 5-HT from 5-HTPLP01. Neuromodulators like 5-HT may disinhibit specific OGs, allowing responses to higher spatial and temporal frequencies, increasing response strength and sensitivity in the VLP, thereby extending the dynamic range of

the feature detector. This phasic effect likely fluctuates with the internal and behavioral state of the animal, especially during changes in locomotion and escape behavior (Aimon et al. 2023; Howard et al. 2019). Serotonin unexpectedly caused a selective Ca^{2+} increase in only the faster velocity OFF bars, normalizing object movement velocity (Figure 4D). Angular velocity information about an expanding loom and its functional relevance to takeoff behavior have been shown in the looming-sensitive LC4 (Ache et al. 2019; von Reyn et al. 2017). Taken together with our findings suggest that presynaptic VPN responses can be sculpted and modulated at the OG, and the LC receptor expression profile is not necessarily indicative of that cell's neuromodulatory potential.

Similarities with olfactory feature detection

Our findings suggest functional similarity to the antennal lobe, another glomerular neuropil of the *Drosophila* brain that encodes olfactory features (Sizemore and Dacks 2016). The effects of 5-HT on the olfactory receptor neuron (ORN) to projection neuron (PN) synapse and on lateral GABAergic inhibition has been much closer examined here (Dacks et al. 2009; Wang 2012; Zhang and Gaudry 2016). The antennal lobe, homologous to the mammalian olfactory bulb, has a diversity of GABAergic local neurons (LNs) that interact with the ORN and PN cells, shaping activity (Chou et al. 2010; Hong and Wilson 2015; Huang et al. 2010; Liu and Wilson 2013; Nagel et al. 2014; Olsen et al. 2010; Olsen and Wilson 2008; Root et al. 2008, 2011; Wilson et al. 2004; Wilson and Laurent 2005; Yaksi and Wilson 2010). The similarities in anatomical architecture between these two neuropils has previously been noted (Mu et al. 2012; Strausfeld et al. 2007).

The mAL neurons are *fru*+ sexually-dimorphic GABAergic cells located in the medial antennal lobe that have been implicated in pheromone sensing and aggression (Kimura et al. 2005; Sengupta and Kravitz 2025). Activation of mAL significantly increases intermale aggression and the phenotype was significantly reduced when GABA release was attenuated in mAL (Sengupta et al. 2022). Different mAL neurons have been shown to be necessary for maintaining a 'gain control' mechanism over P1 neurons and activation of mAL neurons have been shown to suppress male courtship behavior (Clowney et al. 2015). The mALB4 neuron, similarly to mAL, has input synapses in the GNG but instead of ramifying in the superior protocerebrum, mALB4 sends 344 inhibitory synapses onto partners in the PVLP where it could operate as a gain control mechanism across multiple OG in the PVLP (Figure 6C). The 5-HTR expression profile of mALB4 is unknown but, as a GABAergic mAL neuron, expression of 5-HT7 suggests that 5-HT would boost responses in these inhibitory neurons (Mallick et al. 2024). If 5-HT is available in the PVLP extracellular space, mALB4 activation would strongly inhibit PVLP101b and PVLP103, thereby releasing LC15 from feedback inhibition specifically at the glomerulus (Figure 6A). This would allow LC15 to respond to faster velocity OFF bars and motion-defined stimuli.

Activation of mALB4 would turn down the inhibitory tone provided by the GABAergic lateral neurons innervating the LC15 glomerulus (Figure S5A). mALB4 receives input from ascending AN-GNG neurons in the SEZ but these particular ANs have not been physiologically examined. A previous report demonstrated that sucrose stimulation of proboscis gustatory neurons activated the dense and diffuse arborizations of the SEZ 5-HT neurons (Yao and Scott 2022).

An ascending gustatory sugar signal from the SEZ 5-HT neurons could activate mALB4 and release LC15 from inhibition to help facilitate multisensory integration. Previous studies have implicated 5-HT in the modulation of feeding behavior so this ascending signal from the gustatory center may help to orchestrate state-dependent behavior (Albin et al. 2015; Tierney 2020).

Serotonergic motor control and behavioral implications

Serotonin is known to mediate walking in *Drosophila*: 5-HTergic neurons in the VNC slows walking speed, whereas inhibition of those neurons increases it. 5-HT^{VNC} neurons are active during locomotion, positively correlated to the animal's velocity. A previous report tested null receptor mutants and implicated 5-HT7 as the receptor responsible (Howard et al. 2019). Additionally, it has been reported that serotonergic cells in the VNC mediate immobility and the immobility locomotor behavior is mediated by 5-HT7 (Gowda et al. 2023). If an ascending locomotor 'stop' signal from the GNG activates mALB4, this could release LC15 from inhibition coordinated synchronously with the volumetric release of 5-HT from 5-HTPLP, facilitating motion-defined features and normalizing object velocity responses in the stationary animal. By contrast, AN-GNG89 neurons could be active during locomotion and, through mALB4, release LC15 from inhibition in the absence of extracellular 5-HT. Locomotion could activate descending neurons like DNp27 that would activate LmA2, providing inhibitory tone to LC15 at the lobula. At cessation, the mALB4 neurons are no longer activated by ANs, and the PVLP101b and PVLP103 neurons are free to inhibit LC15 at the glomerulus. 5-HTPLP01 neurons are released from suppression and release 5-HT into the PVLP while 5-HT release is reduced elsewhere in the brain. 5-HTPLP01 is strongly innervated by a glutamatergic partner, PVLP106, which shows reciprocal connections and could inhibit 5-HTPLP01 from releasing 5-HT during locomotion but similarly inhibited by glutamate when 5-HTPLP01 is active (Figure S3C). This increase in inhibitory tone could sharpen the features in the visual scene upon cessation of locomotion.

Serotonin acts as both a synaptic neurotransmitter and an extrinsic neuromodulator in invertebrate and vertebrate systems. 5-HT acts via ionotropic signaling by binding to and opening ion channels in the postsynaptic sites of target cells (Rosikon et al. 2023). Additionally, 5-HT acts upon metabotropically by binding to receptors in the cell membranes of a local extracellular space, activating GPCR cascades in multiple heterogeneous cell types. There is a large body of literature on functional mechanisms of serotonergic neurotransmission for both vertebrates and invertebrates, but the neurohormonal mechanisms of 5-HT is critically understudied. The flexibility that 5-HT provides to sensory and motor circuits and the overall contribution of paracrine signaling to serotonergic signaling is unknown.

In both cases of synaptic and paracrine signaling, we know that 5-HT shifts the excitation-inhibition relationship at critical behavioral moments. Inhibitory regulation of circuit elements by 5-HT is not exclusive to fruit flies. In locusts, 5-HT is responsible for the state change from the solitary to gregarious swarming phase, triggering phenotypic, behavioral, and physiological changes in the object-detecting descending contralateral motion detector (DCMD) (Anstey et al. 2009; Matheson et al. 2004). In crabs, upon eliminating this input to the A1 cells, the spontaneous firing rates of 5-HT cells are increased by about 50%, suggesting that these

cells are under constant inhibitory regulation (Edwards and Kravitz 1997; Weiger and Ma 1993). In crayfish, pressure injection of 5-HT causes spatially-segregated inhibitory effects synaptically and excitatory effects through paracrine action on a motor neuron (Bacqué-Cazenave et al. 2013). In the visual cortex of mice, it was observed that visual stimulation with a light flash triggers excitatory and inhibitory conductances that are staggered by a few milliseconds (Liu et al. 2010). Upon visual feature presentation, the ratio between excitation and inhibition is initially tilted toward excitation, and subsequently shifts toward inhibition. The rapid change in the excitation-inhibition ratio plays a critical role in spatial and temporal response tuning. It has previously been demonstrated in vertebrates that oriented OFF bars in the visual field (Anderson et al. 2000; Monier et al. 2003) lead to the concomitant occurrence of synaptic excitation and inhibition in sensory cortices (also see Isaacson and Scanziani 2011). Future research on the distribution of 5-HT receptors, as well as the function of each receptor on each LC, would be required to resolve these outstanding issues and propel our understanding of mechanisms of neuromodulatory action on visual processing.

Glossary

5-HT	serotonin, 5-hydroxytryptamine
5-HTR	serotonin receptor
AVLP	anterior ventrolateral protocerebrum
CPG	central pattern generator
GABA	γ-aminobutyric acid
GNG	gnathal ganglion
GPCR	G protein-coupled receptor
La	lamina
LC	lobula columnar cells
Lo	lobula
LN	lateral neuron
LP	lobula plate
Me	medulla
OG	optic glomerulus
ORN	olfactory receptor neuron
PVLP	posterior ventrolateral protocerebrum
PN	projection neurons
SEZ	subesophageal zone
Trh	tryptophan hydroxylase
VPN	visual projection neuron

Data availability

Source data for this study are available upon request.

Supplemental material

Supplemental information may be found online at <url>.

Competing interests

The authors declare no competing interests.

Acknowledgements

The authors thank SL Bonanno and DE Krantz for helpful discussions and reagents.

Grants

This project was supported by National Institute of Neurological Disorders and Stroke R01NS120984 to MAF.

Disclosures

No conflicts of interest, financial or otherwise, are declared by the authors.

Author contributions

DJB designed the experiments, performed imaging experiments, wrote analysis code, analyzed data, interpreted results, prepared figures, and wrote the manuscript. LMPC provided genetics assistance, and edited the manuscript. MAF acquired funding, conceived of the scope of work, designed experiments, provided supervision, and wrote the manuscript.

Supplemental Figures

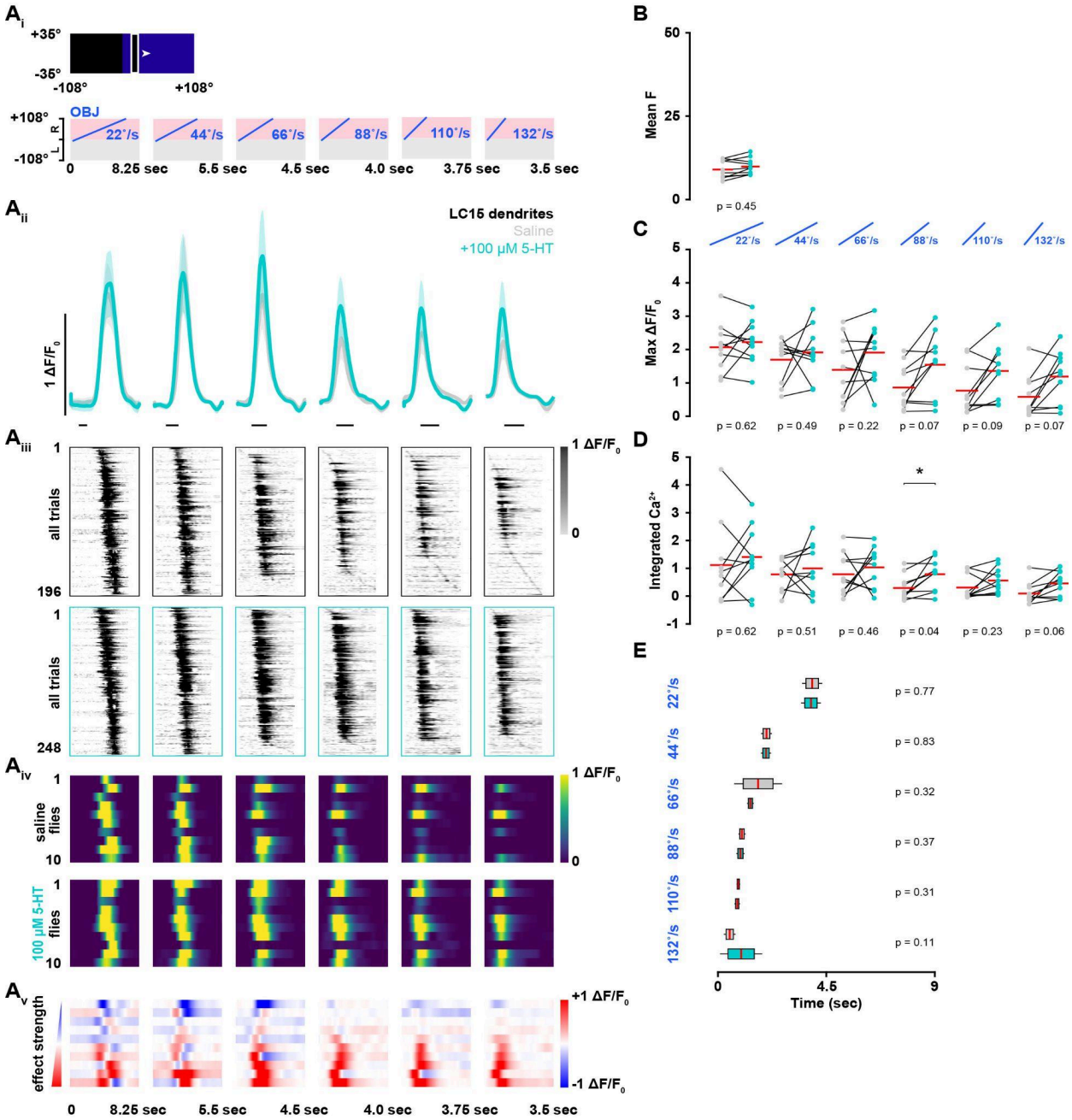

Figure S1. 5-HT recruits individual LC15 dendrites in response to high velocity OFF bars

(Ai) Schematic illustrating the 8.8° x 70° vertical bar presented on the LED display (top) and the motion of the translating feature over time (bottom). The OFF bar moved at six different velocities (22, 44, 66, 88, 110, and 132 °/sec) across the right side of the LED display.

(Aii) Population mean GCaMP6f signal from the LC15 dendrites (± SEM shading) before (gray) and after 100 µM 5-HT (cyan). The vertical scale bar (black) represents 1 $\Delta F/F_0$. The horizontal scale bar (black) represents 1 second.

(Aiii) $\Delta F/F_0$ response raster plots displaying individual trial responses from all ROIs. Two repeats of each stimulus were shown to each animal before (N = 10, n = 196) and after 100 μM 5-HT (n = 248). The trial responses are sorted by the time of the peak $\Delta F/F_0$ response.
(Aiv) $\Delta F/F_0$ response raster plots displaying mean animal responses before (top) and after 100 μM 5-HT (bottom) (N = 10). Flies 1-10 (rows) are sorted the same in the pre-5-HT (top) and post-5-HT (bottom) condition rasters. The bottom row of each raster shows the population mean, denoted with Σ. The vertical red line represents the mean time of the $\Delta F/F_0$ peaks, the box indicates the peak of the $\Delta F/F_0$ mean trace.
(Av) Mean change in effect size rasters of LC15 dendrites GCaMP6f responses for each animal in the saline to the 5-HT experimental group. Animals (row) are sorted by increasing effect size strength. The bottom row of each raster shows the change in the population mean, denoted with Σ. The vertical red line represents the mean time of the $\Delta F/F_0$ peaks, and the vertical blue line represents the mean time of the $\Delta F/F_0$ troughs.The red box indicates the peak of the $\Delta F/F_0$ mean trace and the blue box indicates the trough of the $\Delta F/F_0$ mean trace.
(B) Pairwise comparison of mean fluorescent intensity in the LC15 glomerulus before (gray) and after 100 μM 5-HT (cyan). Horizontal red lines correspond to the population means. Two-tailed paired t-test, N = 10. Saline mean F = 9.3 ±2.7F. 5-HT mean F = 10.2 ±2.4F. p = 0.45951. Mean time lapse between pre- and post- conditions = +40 minutes.
(C) Pairwise comparison of maximum $\Delta F/F_0$ responses in the LC15 glomerulus before (gray) and after 100 μM 5-HT (cyan). Two-tailed paired t-test, N = 10. Saline mean responses: 2.08 ±0.75, 1.70 ±0.64, 1.40 ±0.97, 0.87 ±0.67, 0.77 ±0.74, and 0.59 ±0.64 $\Delta F/F_0$. 5-HT mean responses: 2.23 ±0.64, 1.92 ±0.76, 1.92 ±0.88, 1.55 ±0.95, 1.36 ±0.74, and 1.20 ±0.78 $\Delta F/F_0$. p = 0.62493; p = 0.49094; p = 0.22677; p = 0.079596; p = 0.099429; p = 0.070617.
(D) Pairwise comparison of integrated Ca^{2+} responses in the LC15 glomerulus before (gray) and after 100 μM 5-HT (cyan). Two-tailed paired t-test, N = 10. Saline mean responses: 1.16 ±1.49, 0.82 ±0.54, 0.82 ±0.75, 0.33 ±0.45, 0.35 ±0.46, and 0.13 ±0.40. 5-HT mean responses: 1.45 ±1.12, 1.04 ±0.88, 1.07 ±0.74, 0.83 ±0.56, 0.60 ±0.46, and 0.49 ±0.44. p = 0.62567; p = 0.51522; p = 0.46189; p = 0.044255*; p = 0.23225; p = 0.069583.
(E) Pairwise comparison of time to half-max (sec) for LC15 glomerulus responses before (gray) and after 100 μM 5-HT (cyan). Two-tailed paired t-test, N = 10. Saline mean responses: 3.9 ±0.4, 2.0 ±0.2, 1.7 ±1.0, 1.0 ±0.2, 0.9 ±0.1, and 0.5 ±0.3 seconds. 5-HT mean responses: 3.9 ±0.4, 2.0 ±0.2, 1.4 ±0.2, 0.9 ±0.2, 0.8 ±0.1, and 1.0 ±0.9 seconds. p = 0.77929; p = 0.83323; p = 0.3271; p = 0.37659; p = 0.31123; p = 0.11728.

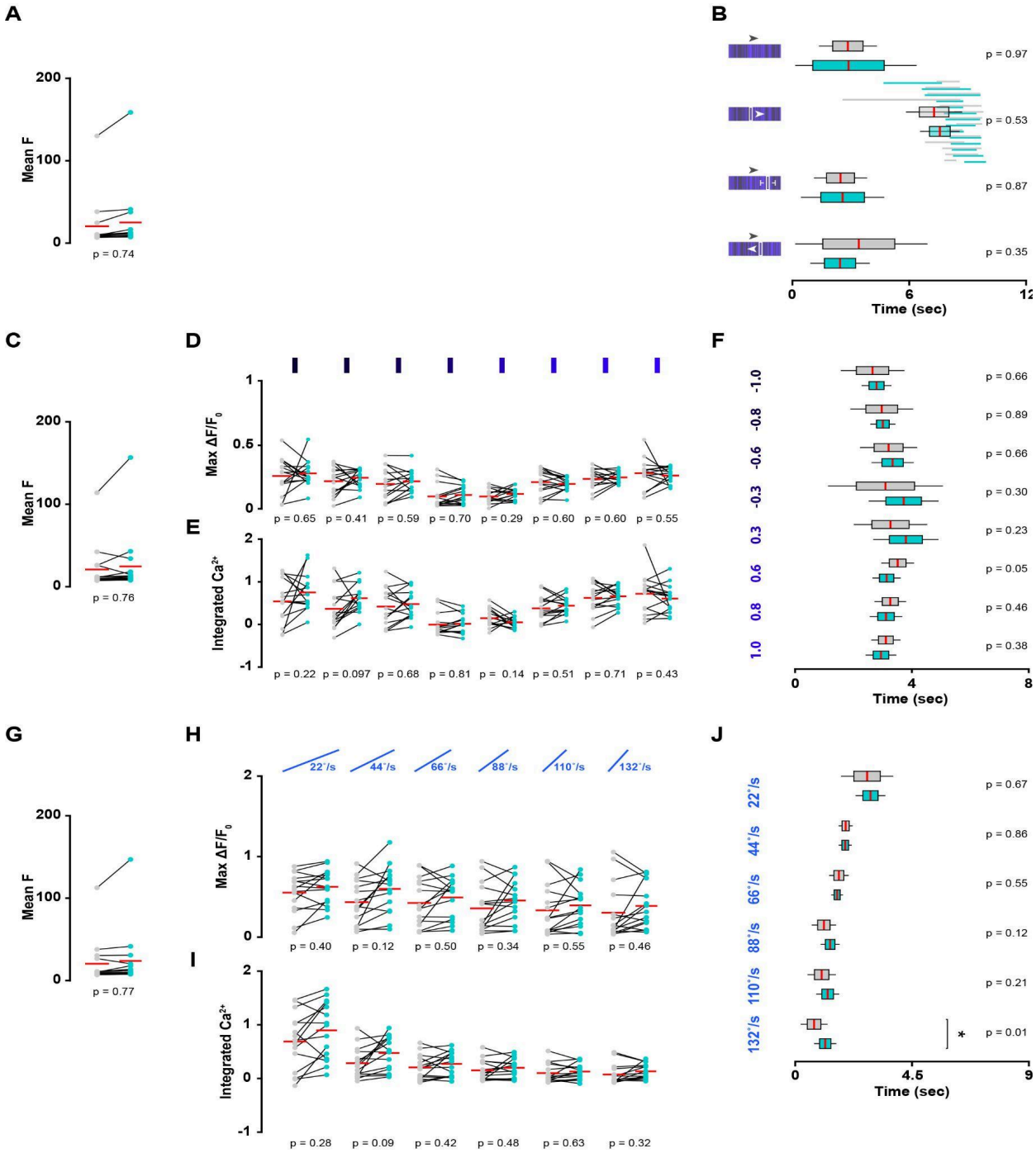

Figure S2. Accompanying statistics for Figure 5.

(A) Pairwise comparison of mean fluorescent intensity in the LC12 glomerulus before (gray) and after 100 μM 5-HT (cyan). Horizontal red lines correspond to the population means. Two-tailed paired t-test, N = 14. Saline mean F = 20.5 ± 32.7F. 5-HT mean F = 25.1 ± 39.9F. p = 0.74341. Mean time lapse between pre- and post- conditions = +39 minutes.

(B) Pairwise comparison of time to half-max (sec) for LC12 glomerular responses before (gray) and after 100 μM 5-HT (cyan). Two-tailed paired t-test, N = 14. Saline mean responses: 2.7 ±1.5, 7.1 ±1.5, 2.3 ±1.4, and 3.3 ±3.5 seconds. 5-HT mean responses: 2.7 ± 3.5, 7.4 ± 1.0, 2.4 ± 2.1, and 2.3 ±1.5 seconds. p = 0.97536; p = 0.53507; p = 0.87825; p = 0.35728. The horizontal lines behind the box plots in the motion-defined bar condition indicate the time

period from the half-max to the maximum $\Delta F/F_0$ responses for each animal before (gray) and after 100 μM 5-HT (cyan).

(C) Pairwise comparison of mean fluorescent intensity in the LC12 dendrites before (gray) and after 100 μM 5-HT (cyan). Horizontal red lines correspond to the population means. Two-tailed paired t-test, N = 15. Saline mean F = 20.9 ±27.6F. 5-HT mean F = 24.6 ±37.9F. p = 0.76034. Mean time lapse between pre- and post- conditions = +38 minutes.

(D) Pairwise comparison of maximum $\Delta F/F_0$ responses in the LC12 glomerulus before (gray) and after 100 μM 5-HT (cyan). Two-tailed paired t-test, N = 15. Saline mean responses: 0.26 ±0.14, 0.22 ±0.11, 0.20 ±0.12, 0.10 ±0.09, 0.10 ±0.05, 0.21 ± 0.09, 0.24 ±0.08, and 0.28 ±0.11 $\Delta F/F_0$. 5-HT mean responses: 0.28 ±0.10, 0.25 ±0.07, 0.22 ±0.08, 0.11 ±0.07, 0.12 ±0.05, 0.20 ±0.05, 0.25 ±0.04, and 0.26 ±0.06 $\Delta F/F_0$. p = 0.65388; p = 0.419; p = 0.59623; p = 0.70333; p = 0.29775; p = 0.6008; p = 0.60734; p = 0.55675.

(E) Pairwise comparison of integrated Ca^{2+} responses in the LC12 glomerulus before (gray) and after 100 μM 5-HT (cyan). Two-tailed paired t-test, N = 15. Saline mean responses: 0.54 ±0.51, 0.37 ±0.47, 0.42 ±0.44, -0.01 ±0.26, 0.15 ±0.21, 0.38 ±0.30, 0.62 ±0.34, and 0.72 ±0.46. 5-HT mean responses: 0.75 ±0.43, 0.62 ±0.32, 0.48 ±0.33, 0.02 ±0.21, 0.05 ±0.13, 0.44 ±0.20, 0.66 ±0.21, and 0.61 ±0.32. p = 0.22942; p = 0.097839; p = 0.68063; p = 0.81441; p = 0.14218; p = 0.51476; p = 0.71213; p = 0.43841.

(F) Pairwise comparison of time to half-max (sec) for LC12 glomerulus responses before (gray) and after 100 μM 5-HT (cyan). Two-tailed paired t-test, N = 15. Saline mean responses: 2.65 ±1.09, 2.96 ±1.07, 3.20 ±0.98, 3.09 ±1.97, 3.26 ±1.26, 3.51 ±0.56, 3.26 ±0.54, and 3.10 ±0.50 seconds. 5-HT mean responses: 2.78 ±0.51, 3.00 ±0.43, 3.34 ±0.72, 3.71 ±1.20, 3.79 ±1.12, 3.13 ±0.49, 3.11 ±0.56, and 2.94 ±0.53 seconds. p = 0.66706; p = 0.89636; p = 0.66549; p = 0.30449; p = 0.23448; p = 0.058331; p = 0.46895; p = 0.38026.

(G) Pairwise comparison of mean fluorescent intensity in the LC12 glomerulus before (gray) and after 100 μM 5-HT (cyan). Two-tailed paired t-test, N = 15. Saline mean F = 20.4 ±27.2F. 5-HT mean F = 23.8 ±35.4F. p = 0.77095. Mean time lapse between pre- and post- conditions = +38 minutes.

(H) Pairwise comparison of maximum $\Delta F/F_0$ responses in the LC12 glomerulus before (gray) and after 100 μM 5-HT (cyan). Two-tailed paired t-test, N = 15. Saline mean responses: 0.28 ±0.12, 0.22 ±0.14, 0.21 ±0.15, 0.18 ±0.15, 0.17 ±0.16, and 0.15 ±0.17 $\Delta F/F_0$. 5-HT mean responses: 0.31 ±0.11, 0.30 ±0.15, 0.25 ±0.13, 0.23 ±0.13, 0.20 ±0.13, and 0.19 ±0.14 $\Delta F/F_0$. p = 0.40072; p = 0.1233; p = 0.50841; p = 0.34823; p = 0.55249; p = 0.46837.

(I) Pairwise comparison of integrated Ca^{2+} responses in the LC12 glomerulus before (gray) and after 100 μM 5-HT (cyan). Two-tailed paired t-test, N = 15. Saline mean responses: 0.69 ±0.53, 0.28 ±0.29, 0.21 ±0.23, 0.15 ±0.19, 0.10 ±0.18, and 0.07 ±0.19. 5-HT mean responses: 0.90 ±0.53, 0.47 ±0.31, 0.27 ±0.22, 0.20 ±0.18, 0.13 ±0.15, and 0.13 ±0.14. p = 0.28879; p = 0.090397; p = 0.42695; p = 0.4842; p = 0.63555; p = 0.32845.

(J) Pairwise comparison of time to half-max (sec) for LC12 glomerulus responses before (gray) and after 100 μM 5-HT (cyan). Two-tailed paired t-test, N = 15. Saline mean responses: 2.8 ±1.0, 1.9 ±0.3, 1.7 ±0.4, 1.1 ±0.5, 1.0 ±0.6, and 0.7 ±0.5 seconds. 5-HT mean responses: 2.9 ±0.6, 1.9 ±0.3, 1.6 ±0.2, 1.4 ±0.4, 1.3 ±0.4, and 1.2 ±0.4 seconds. p = 0.67116; p = 0.86005; p = 0.55694; p = 0.12728; p = 0.21319; p = 0.019491*.

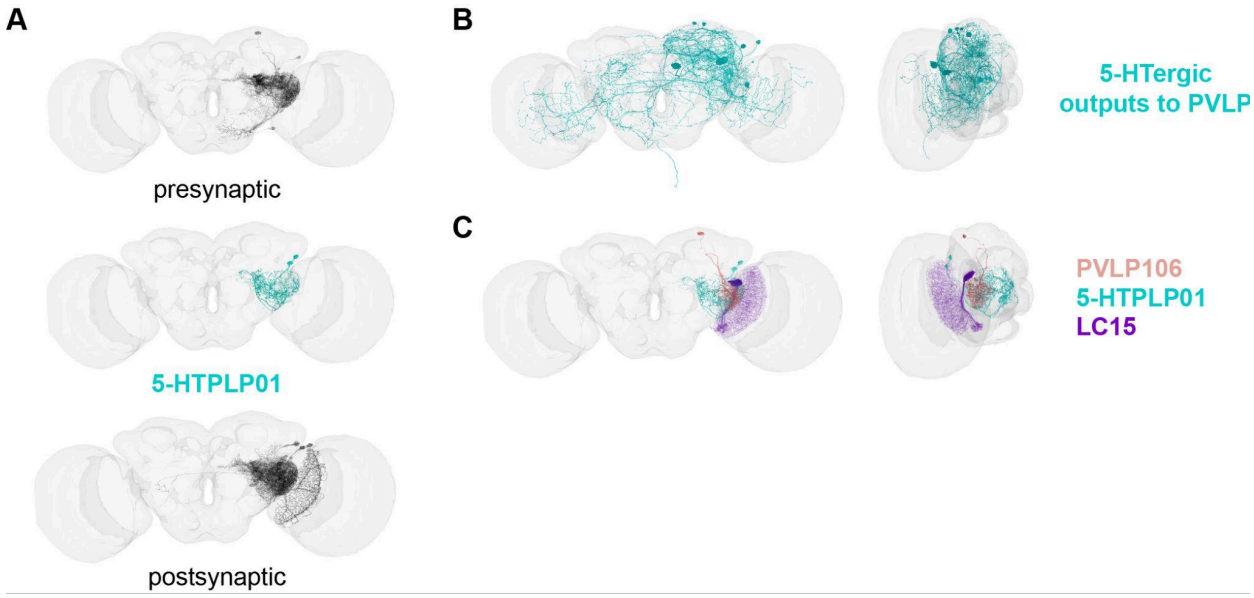

Figure S3. Serotonergic innervation of the PVLP

(A) Presynaptic partners (black, top) to 5-HTPLP (cyan) and postsynaptic partners (black, bottom) in the right hemisphere.

(B) Serotonergic neurons (cyan) that have output synapses in the right hemisphere PVLP.

(C) Morphology of PVLP106, a glutamatergic interneuron that has reciprocal synapses onto 5-HTPLP01 (cyan). LC15 (purple) does not make synapses with either group.

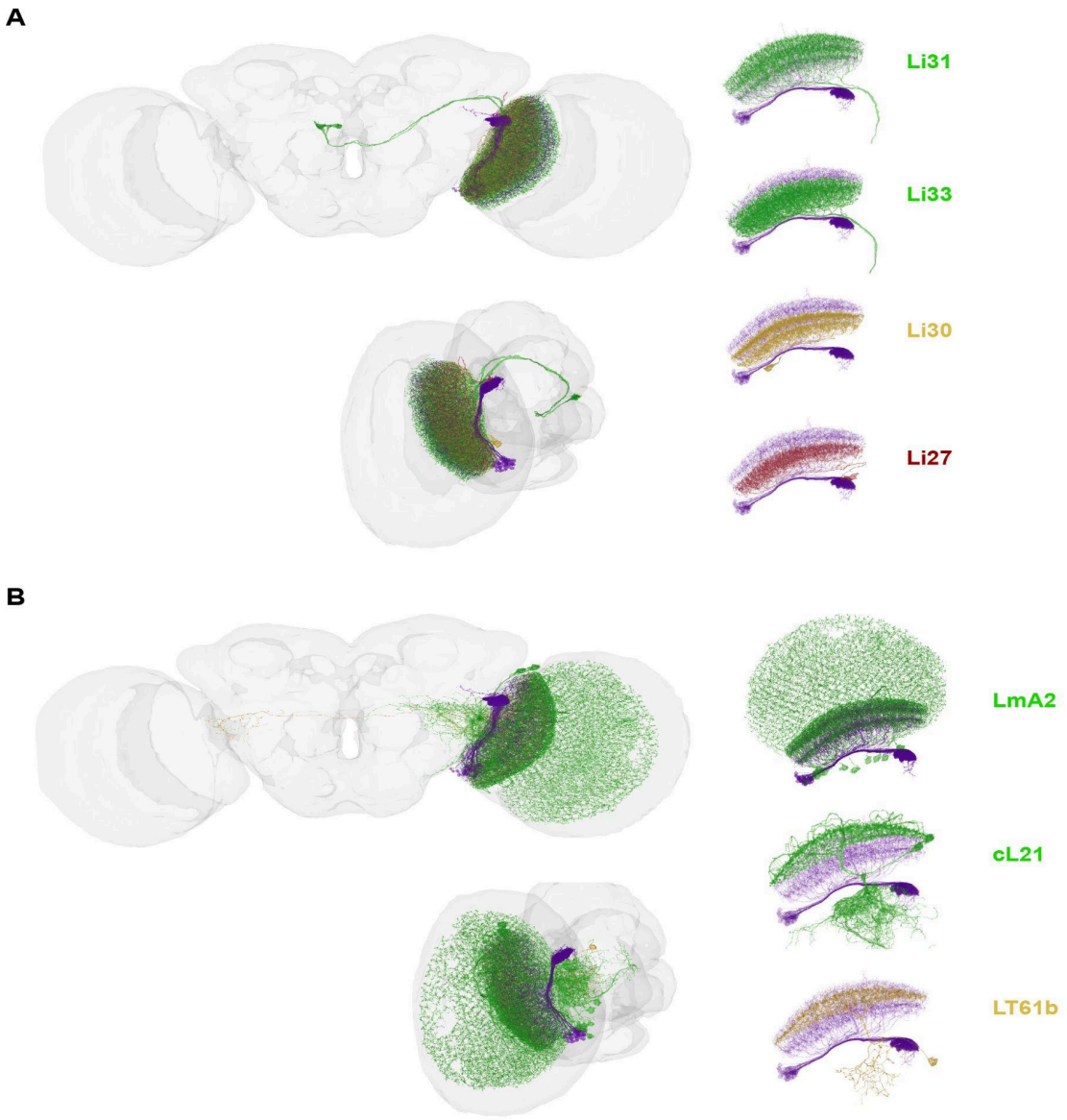

Figure S4. LC15 inhibitory circuit motifs in the optic lobe

(A) Morphology reconstruction of Li30-Li31-Li33-Li27 circuit motif. LC15 (purple) is shown for reference. The neurons are colored according to neurotransmitter type (yellow, cholinergic) (green, GABAergic) (red, glutamatergic).

(B) Morphology reconstruction of LT61b-cL21-LmA2 circuit motif. LC15 (purple) is shown for reference. The neurons are colored according to neurotransmitter type (yellow, cholinergic) (green, GABAergic). The centrifugal GABAergic neurons, cL21, is the highest downstream partner of 5-HTPLP01, making over 700 glutamatergic synapses. In the lobula, inhibition of cL21 would release LmA2 neurons from GABAergic inhibition, causing a stronger inhibitory suppression on LC15 at the lobula. Glutamatergic suppression of cL21 would also release T2 and T3 from inhibition at the lobula, possibly causing a potentiation of small objects in other LCs. Opposingly, LT61b, a cholinergic output of LC15, sends excitatory signals from the VLP on both hemispheres to cL21 in the lobula. Activation of cL21 by LT61b would strengthen the GABAergic inhibition of cL21 over LmA2 and release LC15 ‘s dendrites from inhibition.

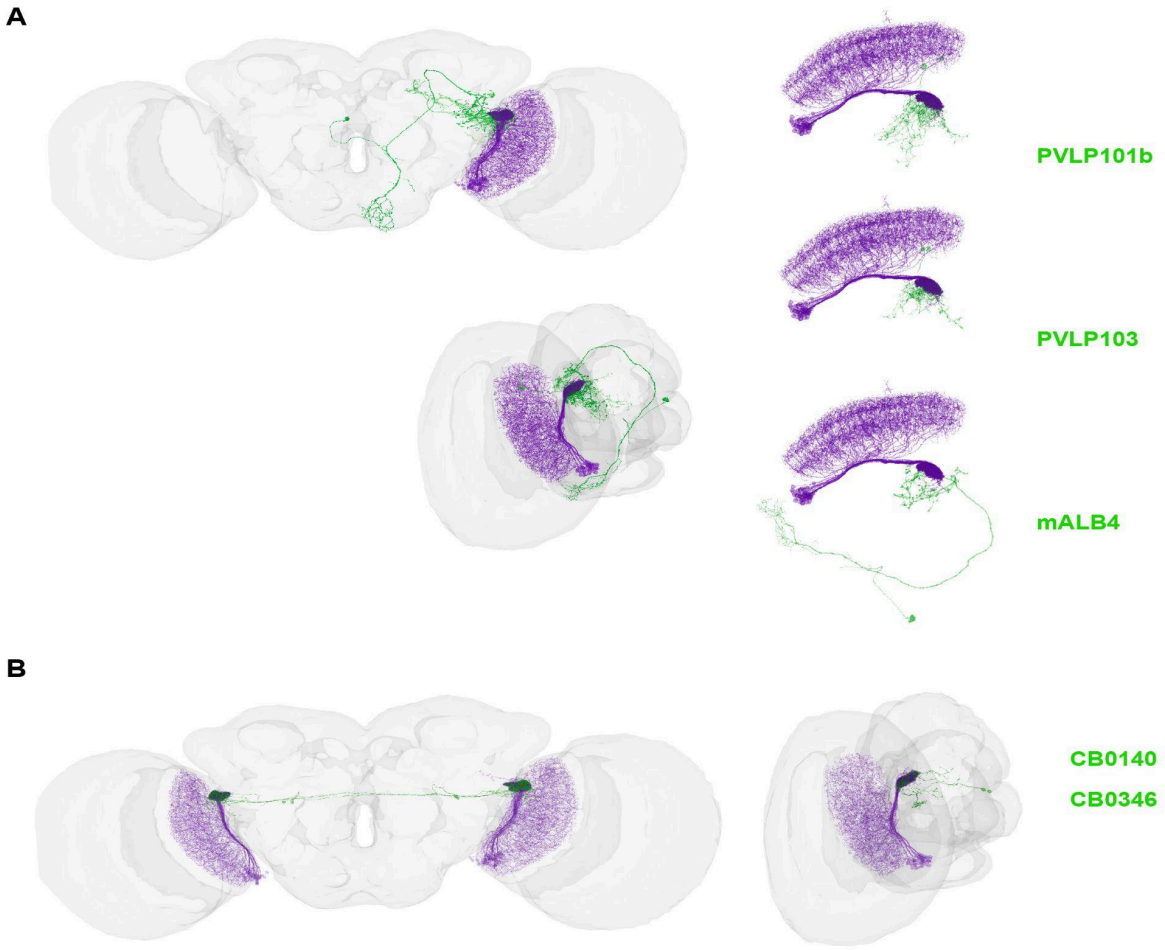

Figure S5. LC15 inhibitory circuit motifs in the central brain

(A) Morphology reconstruction of mALB4-PVLP101b-PVLP103 circuit motif. LC15 (purple) is shown for reference. The neurons are colored according to neurotransmitter type (green, GABAergic).

(B) Morphology reconstruction of CB0140-CB0346 circuit motif. LC15 (purple) is shown for reference. The neurons are colored according to neurotransmitter type (green, GABAergic).

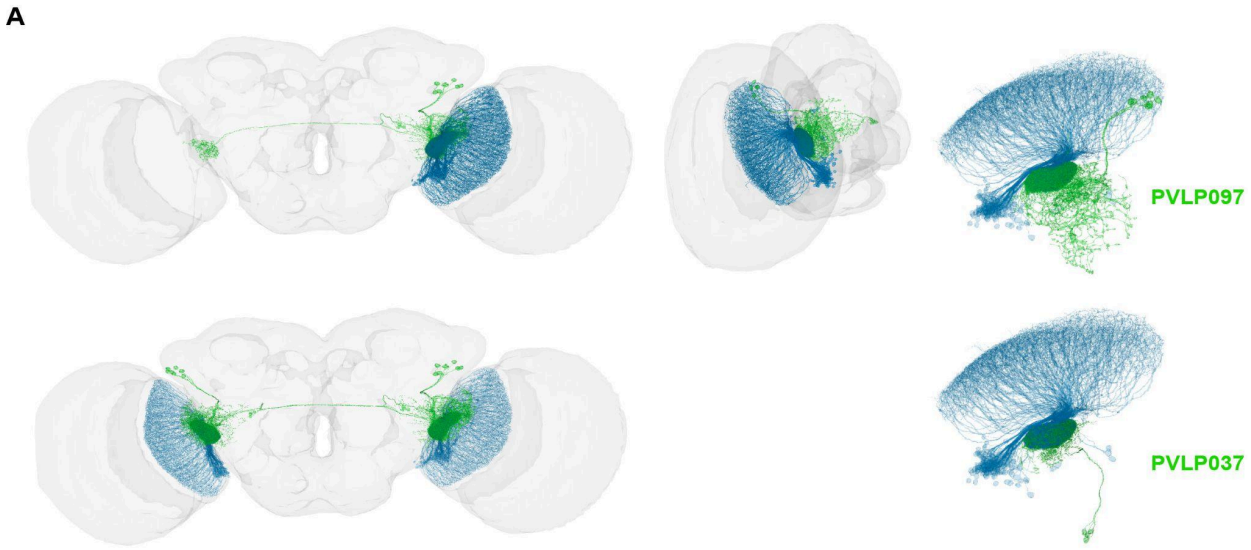

Figure S6. LC12 axo-axonal inhibitory circuit motif

(A) Morphology reconstruction of PVLP037-PVLP097 circuit motif. LC12 (blue) is shown for reference in one hemisphere (left, top), and bilaterally (left, bottom). The neurons are colored according to neurotransmitter type (green, GABAergic). This circuit motif is reminiscent of what has previously been reported in other LCs (Morimoto et al. 2020; Schretter et al. 2024). There are 7 PVLP097 cells that make over 2,000 GABAergic synapses back onto LC12. High inhibitory tone from PVLP097 likely contributes to 'weak' glomerular responses from LC12 compared to previous reports that imaged in the lobula dendrites. Instead of direct axo-axonic LC12-LC12 connections by a GABAergic lateral neuron, the PVLP037 cells make 684 GABAergic synapses onto PVLP097. If PVLP037 is a state-dependent neuron, it could mediate a switch for context-specific LC12 feature sensitivity. For example, flight could activate PVLP037 and release LC12 from inhibition to better respond to a vertical bar, or looming stimulus. Removing the PVLP097 cells should expand the feature-detection parameter space in LC12 and activating PVLP037 may recapitulate that effect.

References

Ache JM, **Polsky J**, **Alghailani S**, **Parekh R**, **Breads P**, **Peek MY**, **Bock DD**, **von Reyn CR**, **Card GM**. Neural basis for looming size and velocity encoding in the Drosophila giant fiber escape pathway. *Curr Biol* 29: 1073–1081.e4, 2019.

Aimon S, **Cheng KY**, **Gjorgjieva J**, **Grunwald Kadow IC**. Global change in brain state during spontaneous and forced walk in is composed of combined activity patterns of different neuron classes. *Elife* 12, 2023.

Albin SD, **Kaun KR**, **Knapp J-M**, **Chung P**, **Heberlein U**, **Simpson JH**. A subset of serotonergic neurons evokes hunger in adult Drosophila. *Curr Biol* 25: 2435–2440, 2015.

Alekseyenko OV, **Chan Y-B**, **Okaty BW**, **Chang Y**, **Dymecki SM**, **Kravitz EA**. Serotonergic Modulation of Aggression in Drosophila Involves GABAergic and Cholinergic Opposing Pathways. *Curr Biol* 29: 2145–2156.e5, 2019.

Alekseyenko OV, **Kravitz EA**. Serotonin and the search for the anatomical substrate of aggression. *Fly (Austin)* 8: 200–205, 2014.

Anderson JS, **Carandini M**, **Ferster D**. Orientation tuning of input conductance, excitation, and inhibition in cat primary visual cortex. *J Neurophysiol* 84: 909–926, 2000.

Anstey ML, **Rogers SM**, **Ott SR**, **Burrows M**, **Simpson SJ**. Serotonin mediates behavioral gregarization underlying swarm formation in desert locusts. *Science* 323: 627–630, 2009.

Aptekar JW, **Keleş MF**, **Lu PM**, **Zolotova NM**, **Frye MA**. Neurons forming optic glomeruli compute figure-ground discriminations in Drosophila. *J Neurosci* 35: 7587–7599, 2015.

Bacqué-Cazenave J, **Issa FA**, **Edwards DH**, **Cattaert D**. Spatial segregation of excitatory and inhibitory effects of 5-HT on crayfish motoneurons. *J Neurophysiol* 109: 2793–2802, 2013.

Becnel J, **Johnson O**, **Luo J**, **Nässel DR**, **Nichols CD**. The serotonin 5-HT7Dro receptor is expressed in the brain of Drosophila, and is essential for normal courtship and mating. *PLoS One* 6: e20800, 2011.

Behnia R, **Clark DA**, **Carter AG**, **Clandinin TR**, **Desplan C**. Processing properties of ON and OFF pathways for Drosophila motion detection. *Nature* 512: 427–430, 2014.

Blenau W, **Baumann A**. Molecular and pharmacological properties of insect biogenic amine receptors: lessons from Drosophila melanogaster and Apis mellifera. *Arch Insect Biochem Physiol* 48: 13–38, 2001.

Blenau W, **Thamm M**. Distribution of serotonin (5-HT) and its receptors in the insect brain with focus on the mushroom bodies: lessons from Drosophila melanogaster and Apis mellifera. *Arthropod Struct Dev* 40: 381–394, 2011.

Bonanno SL, **Sanfilippo P**, **Eamani A**, **Sampson MM**, **Kandagedon B**, **Li K**, **Burns GD**, **Makar ME**, **Zipursky SL**, **Krantz DE**. Constitutive and Conditional Epitope Tagging of Endogenous G-Protein-Coupled Receptors in. *J Neurosci* 44, 2024.

Borst A, **Haag J**, **Mauss AS**. How fly neurons compute the direction of visual motion. *J Comp Physiol A Neuroethol Sens Neural Behav Physiol* 206: 109–124, 2020.

Cheng KY, **Colbath RA**, **Frye MA**. Olfactory and neuromodulatory signals reverse visual object avoidance to approach in Drosophila. *Curr Biol* 29: 2058–2065.e2, 2019.

Chen T-W, **Wardill TJ**, **Sun Y**, **Pulver SR**, **Renninger SL**, **Baohan A**, **Schreiter ER**, **Kerr RA**, **Orger MB**, **Jayaraman V**, **Looger LL**, **Svoboda K**, **Kim DS**. Ultrasensitive fluorescent proteins for imaging neuronal activity. *Nature* 499: 295–300, 2013.

Chou Y-H, **Spletter ML**, **Yaksi E**, **Leong JCS**, **Wilson RI**, **Luo L**. Diversity and wiring variability of olfactory local interneurons in the Drosophila antennal lobe. *Nat Neurosci* 13: 439–449, 2010.

Ciranna L. Serotonin as a modulator of glutamate- and GABA-mediated neurotransmission: implications in physiological functions and in pathology. *Curr Neuropharmacol* 4: 101–114, 2006.

Clowney EJ, **Iguchi S**, **Bussell JJ**, **Scheer E**, **Ruta V**. Multimodal Chemosensory Circuits

Controlling Male Courtship in Drosophila. *Neuron* 87: 1036–1049, 2015.

Dacks AM, **Green DS**, **Root CM**, **Nighorn AJ**, **Wang JW**. Serotonin modulates olfactory processing in the antennal lobe of Drosophila. *J Neurogenet* 23: 366–377, 2009.

Dierick HA, **Greenspan RJ**. Serotonin and neuropeptide F have opposite modulatory effects on fly aggression. *Nat Genet* 39: 678–682, 2007.

Dorkenwald S, **Matsliah A**, **Sterling AR**, **Schlegel P**, **Yu S-C**, **McKellar CE**, **Lin A**, **Costa M**, **Eichler K**, **Yin Y**, **Silversmith W**, **Schneider-Mizell C**, **Jordan CS**, **Brittain D**, **Halageri A**, **Kuehner K**, **Ogedengbe O**, **Morey R**, **Gager J**, **Kruk K**, **Perlman E**, **Yang R**, **Deutsch D**, **Bland D**, **Sorek M**, **Lu R**, **Macrina T**, **Lee K**, **Bae JA**, **Mu S**, **Nehoran B**, **Mitchell E**, **Popovych S**, **Wu J**, **Jia Z**, **Castro MA**, **Kemnitz N**, **Ih D**, **Bates AS**, **Eckstein N**, **Funke J**, **Collman F**, **Bock DD**, **Jefferis GSXE**, **Seung HS**, **Murthy M**, **FlyWire Consortium**. Neuronal wiring diagram of an adult brain. *Nature* 634: 124–138, 2024.

Edwards DH, **Kravitz EA**. Serotonin, social status and aggression. *Curr Opin Neurobiol* 7: 812–819, 1997.

El-Kholy S, **Stephano F**, **Li Y**, **Bhandari A**, **Fink C**, **Roeder T**. Expression analysis of octopamine and tyramine receptors in Drosophila. *Cell Tissue Res* 361: 669–684, 2015.

Evans PD, **Maqueira B**. Insect octopamine receptors: a new classification scheme based on studies of cloned Drosophila G-protein coupled receptors. *Invert Neurosci* 5: 111–118, 2005.

Fischbach K-F, **Dittrich APM**. The optic lobe of Drosophila melanogaster. I. A Golgi analysis of wild-type structure. *Cell Tissue Res* 258, 1989.

Fox JL, **Aptekar JW**, **Zolotova NM**, **Shoemaker PA**, **Frye MA**. Figure-ground discrimination behavior in Drosophila. I. Spatial organization of wing-steering responses. *J Exp Biol* 217: 558–569, 2014.

Frighetto G, **Frye MA**. Columnar neurons support saccadic bar tracking in Drosophila. *Elife* 12: e83656, 2023.

Gajardo I, **Guerra S**, **Campusano JM**. Navigating Like a Fly: as a Model to Explore the Contribution of Serotonergic Neurotransmission to Spatial Navigation. *Int J Mol Sci* 24, 2023.

Gasque G, **Conway S**, **Huang J**, **Rao Y**, **Vosshall LB**. Small molecule drug screening in Drosophila identifies the 5HT2A receptor as a feeding modulation target. *Sci Rep* 3: srep02120, 2013.

Gowda SBM, **Banu A**, **Salim S**, **Peker KA**, **Mohammad F**. Serotonin distinctly controls behavioral states in restrained and freely moving Drosophila. *iScience* 26: 105886, 2023.

Hardcastle BJ, **Omoto JJ**, **Kandimalla P**, **Nguyen B-CM**, **Keleş MF**, **Boyd NK**, **Hartenstein V**, **Frye MA**. A visual pathway for skylight polarization processing in. *Elife* 10, 2021.

Hevers W, **Hardie RC**. Serotonin modulates the voltage dependence of delayed rectifier and Shaker potassium channels in Drosophila photoreceptors. *Neuron* 14: 845–856, 1995.

Hong EJ, **Wilson RI**. Simultaneous encoding of odors by channels with diverse sensitivity to inhibition. *Neuron* 85: 573–589, 2015.

Howard CE, **Chen C-L**, **Tabachnik T**, **Hormigo R**, **Ramdya P**, **Mann RS**. Serotonergic modulation of walking in Drosophila. *Curr Biol* 29: 4218–4230.e8, 2019.

Huang J, **Zhang W**, **Qiao W**, **Hu A**, **Wang Z**. Functional connectivity and selective odor responses of excitatory local interneurons in Drosophila antennal lobe. *Neuron* 67: 1021–1033, 2010.

Isaacson JS, **Scanziani M**. How inhibition shapes cortical activity. *Neuron* 72: 231–243, 2011.

Joesch M, **Schnell B**, **Raghu S**, **Reiff D**, **Borst A**. ON and OFF pathways in Drosophila motion vision. *Nature* 468: 300–304, 2010.

Johnson O, **Becnel J**, **Nichols CD**. Serotonin 5-HT1A-like, 5-HT2, and 5-HT7 receptors modulate learning and memory in Drosophila. *FASEB J* 23, 2009.

Johnson O, **Becnel J**, **Nichols CD**. Serotonin receptor activity is necessary for olfactory learning and memory in Drosophila melanogaster. *Neuroscience* 192: 372–381, 2011.

Keleş MF, **Frye MA**. Object-detecting neurons in Drosophila. *Curr Biol* 27: 680–687, 2017.

Keleş MF, **Mongeau J-M**, **Frye MA**. Object features and T4/T5 motion detectors modulate the dynamics of bar tracking by Drosophila. *J Exp Biol* 222: jeb190017, 2019.

Kimura K-I, **Ote M**, **Tazawa T**, **Yamamoto D**. Fruitless specifies sexually dimorphic neural circuitry in the Drosophila brain. *Nature* 438: 229–233, 2005.

Klapoetke NC, **Nern A**, **Rogers EM**, **Rubin GM**, **Reiser MB**, **Card GM**. A functionally ordered visual feature map in the Drosophila brain. *Neuron* 110: 1700–1711.e6, 2022.

Liu B-H, **Li P**, **Sun YJ**, **Li Y-T**, **Zhang LI**, **Tao HW**. Intervening inhibition underlies simple-cell receptive field structure in visual cortex. *Nat Neurosci* 13: 89–96, 2010.

Liu WW, **Wilson RI**. Glutamate is an inhibitory neurotransmitter in the Drosophila olfactory system. *Proc Natl Acad Sci U S A* 110: 10294–10299, 2013.

Maisak MS, **Haag J**, **Ammer G**, **Serbe E**, **Meier M**, **Leonhardt A**, **Schilling T**, **Bahl A**, **Rubin GM**, **Nern A**, **Dickson BJ**, **Reiff DF**, **Hopp E**, **Borst A**. A directional tuning map of Drosophila elementary motion detectors. *Nature* 500: 212–216, 2013.

Majeed ZR, **Abdeljaber E**, **Soveland R**, **Cornwell K**, **Bankemper A**, **Koch F**, **Cooper RL**. Modulatory Action by the Serotonergic System: Behavior and Neurophysiology in Drosophila melanogaster. *Neural Plast* 2016: 7291438, 2016.

Mallick A, **Tan HL**, **Epstein JM**, **Jing Ng CM**, **Cook OM**, **Gaudry Q**, **Dacks AM**. Serotonin acts through multiple cellular targets during an olfactory critical period. *iScience* 27: 111083, 2024.

Matheson T, **Rogers SM**, **Krapp HG**. Plasticity in the visual system is correlated with a change in lifestyle of solitarious and gregarious locusts. *J Neurophysiol* 91: 1–12, 2004.

Monastirioti M. Biogenic amine systems in the fruit fly Drosophila melanogaster. *Microsc Res Tech* 45: 106–121, 1999.

Mongeau J-M, **Frye MA**. Drosophila spatiotemporally integrates visual signals to control saccades. *Curr Biol* 27: 2901–2914.e2, 2017.

Monier C, **Chavane F**, **Baudot P**, **Graham LJ**, **Frégnac Y**. Orientation and direction selectivity of synaptic inputs in visual cortical neurons. *Neuron* 37: 663–680, 2003.

Morimoto MM, **Nern A**, **Zhao A**, **Rogers EM**, **Wong AM**, **Isaacson MD**, **Bock DD**, **Rubin GM**, **Reiser MB**. Spatial readout of visual looming in the central brain of. *Elife* 9, 2020.

Mu L, **Ito K**, **Bacon J**, **Strausfeld N**. Optic glomeruli and their inputs in Drosophila share an organizational ground pattern with the antennal lobes. *J Neurosci* 32: 6061–6071, 2012.

Nagel KI, **Hong EJ**, **Wilson RI**. Synaptic and circuit mechanisms promoting broadband transmission of olfactory stimulus dynamics. *Nat Neurosci* 18: 56–65, 2014.

Namiki S, **Dickinson MH**, **Wong AM**, **Korff W**, **Card GM**. The functional organization of descending sensory-motor pathways in. *Elife* 7, 2018.

Nässel DR. Neuropeptide signaling near and far: how localized and timed is the action of neuropeptides in brain circuits? *Invert Neurosci* 9: 57–75, 2009.

Nässel DR. Substrates for neuronal cotransmission with neuropeptides and small molecule neurotransmitters in Drosophila. *Front Cell Neurosci* 12: 83, 2018.

Nässel DR. What Drosophila can tell us about state-dependent peptidergic signaling in insects. *Insect Biochem Mol Biol* 179: 104275, 2025.

Nässel DR, **Homberg U**. Neuropeptides in interneurons of the insect brain. *Cell Tissue Res* 326: 1–24, 2006.

Olsen SR, **Bhandawat V**, **Wilson RI**. Divisive normalization in olfactory population codes. *Neuron* 66: 287–299, 2010.

Olsen SR, **Wilson RI**. Lateral presynaptic inhibition mediates gain control in an olfactory circuit. *Nature* 452: 956–960, 2008.

Otsuna H, **Ito K**. Systematic analysis of the visual projection neurons of Drosophila melanogaster. I. Lobula-specific pathways. *J Comp Neurol* 497: 928–958, 2006.

Panser K, **Tirian L**, **Schulze F**, **Villalba S**, **Jefferis GSXE**, **Bühler K**, **Straw AD**. Automatic segmentation of Drosophila neural compartments using GAL4 expression data reveals novel visual pathways. *Curr Biol* 26: 1943–1954, 2016.

Pooryasin A, **Fiala A**. Identified Serotonin-Releasing Neurons Induce Behavioral Quiescence and Suppress Mating in Drosophila. *J Neurosci* 35: 12792–12812, 2015.

Qian Y, **Cao Y**, **Deng B**, **Yang G**, **Li J**, **Xu R**, **Zhang D**, **Huang J**, **Rao Y**. Sleep homeostasis regulated by 5HT2b receptor in a small subset of neurons in the dorsal fan-shaped body of drosophila. *Elife* 6: e26519, 2017.

Reiser MB, **Dickinson MH**. A modular display system for insect behavioral neuroscience. *J Neurosci Methods* 167: 127–139, 2008.

von Reyn CR, **Nern A**, **Williamson WR**, **Breads P**, **Wu M**, **Namiki S**, **Card GM**. Feature integration drives probabilistic behavior in the Drosophila escape response. *Neuron* 94: 1190–1204.e6, 2017.

Root CM, **Ko KI**, **Jafari A**, **Wang JW**. Presynaptic facilitation by neuropeptide signaling mediates odor-driven food search. *Cell* 145: 133–144, 2011.

Root CM, **Masuyama K**, **Green DS**, **Enell LE**, **Nässel DR**, **Lee C-H**, **Wang JW**. A presynaptic gain control mechanism fine-tunes olfactory behavior. *Neuron* 59: 311–321, 2008.

Rosikon KD, **Bone MC**, **Lawal HO**. Regulation and modulation of biogenic amine neurotransmission in Drosophila and Caenorhabditis elegans. *Front Physiol* 14: 970405, 2023.

Ryu L, **Kim SY**, **Kim AJ**. From photons to behaviors: Neural implementations of visual behaviors in Drosophila. *Front Neurosci* 16: 883640, 2022.

Sampson MM, **Myers Gschweng KM**, **Hardcastle BJ**, **Bonanno SL**, **Sizemore TR**, **Arnold RC**, **Gao F**, **Dacks AM**, **Frye MA**, **Krantz DE**. Serotonergic modulation of visual neurons in Drosophila melanogaster. *PLoS Genet* 16: e1009003, 2020.

Saudou F, **Boschert U**, **Amlaiky N**, **Plassat JL**, **Hen R**. A family of Drosophila serotonin receptors with distinct intracellular signalling properties and expression patterns. *EMBO J* 11: 7–17, 1992.

Schäfer MK-H, **Varoqui H**, **Defamie N**, **Weihe E**, **Erickson JD**. Molecular cloning and functional identification of mouse vesicular glutamate transporter 3 and its expression in subsets of novel excitatory neurons. *J Biol Chem* 277: 50734–50748, 2002.

Schretter CE, **Sten TH**, **Klapoetke NC**, **Shao M**, **Nern A**, **Dreher M**, **Bushey D**, **Robie A**, **Taylor AL**, **Branson KM**, **Otopalik A**, **Ruta V**, **Rubin GM**. Social state alters vision using three circuit mechanisms in Drosophila. *Nature* 637: 646–653, 2024.

Sengupta S, **Chan Y-B**, **Palavicino-Maggio CB**, **Kravitz EA**. GABA transmission from mAL interneurons regulates aggression in Drosophila males. *Proc Natl Acad Sci U S A* 119: e2117101119, 2022.

Sengupta S, **Kravitz EA**. Decoding sex differences: how GABA shapes Drosophila behavior. *Curr Opin Insect Sci* 67: 101293, 2025.

Seung HS. Predicting visual function by interpreting a neuronal wiring diagram. *Nature* 634: 113–123, 2024.

Shafer OT, **Gutierrez G**, **Li K**, **Mildenhall A**, **Spira D**, **Marty J**, **Lazar A**, **Fernández MP**. Connectomic analysis of the Drosophila lateral neuron clock cells reveals the synaptic basis of functional pacemaker classes. *eLife* 11, 2022.

Sitaraman D, **Zars M**, **Laferriere H**, **Chen Y-C**, **Sable-Smith A**, **Kitamoto T**, **Rottinghaus GE**, **Zars T**. Serotonin is necessary for place memory in Drosophila. *Proc Natl Acad Sci U S A* 105:

5579–5584, 2008.

Sizemore TR, **Dacks AM**. Serotonergic Modulation Differentially Targets Distinct Network Elements within the Antennal Lobe of Drosophila melanogaster. *Sci Rep* 6: 37119, 2016.

Sizemore TR, **Hurley LM**, **Dacks AM**. Serotonergic modulation across sensory modalities. *J Neurophysiol* 123: 2406–2425, 2020.

Städele C, **Keleş MF**, **Mongeau J-M**, **Frye MA**. Non-canonical receptive field properties and neuromodulation of feature-detecting neurons in flies. *Curr Biol* 30: 2508–2519.e6, 2020.

Strausfeld NJ. Atlas of an insect brain [Online]. 20147: 31–54, 1976https://scholar.google.com/citations?view_op=view_citation&hl=en&citation_for_view=Sq3QUCYAAAAJ:u5HHmVD_uO8C.

Strausfeld NJ, **Okamura J-Y**. Visual system of calliphorid flies: organization of optic glomeruli and their lobula complex efferents. *J Comp Neurol* 500: 166–188, 2007.

Strausfeld NJ, **Sinakevitch I**, **Okamura J-Y**. Organization of local interneurons in optic glomeruli of the dipterous visual system and comparisons with the antennal lobes. *Dev Neurobiol* 67: 1267–1288, 2007.

Strother JA, **Nern A**, **Reiser MB**. Direct observation of ON and OFF pathways in the Drosophila visual system. *Curr Biol* 24: 976–983, 2014.

Suzuki Y, **Schenk JE**, **Tan H**, **Gaudry Q**. A population of interneurons signals changes in the basal concentration of serotonin and mediates gain control in the Drosophila antennal lobe. *Curr Biol* 30: 1110–1118.e4, 2020.

Theobald JC, **Duistermars BJ**, **Ringach DL**, **Frye MA**. Flies see second-order motion. *Curr Biol* 18: R464–5, 2008.

Tierney AJ. Feeding, hunger, satiety and serotonin in invertebrates. *Proc Biol Sci* 287: 20201386, 2020.

Turner MH, **Krieger A**, **Pang MM**, **Clandinin TR**. Visual and motor signatures of locomotion dynamically shape a population code for feature detection in. *Elife* 11, 2022.

Vleugels R, **Verlinden H**, **Broeck J**. Serotonin, serotonin receptors and their actions in insects. *Neurotransmitter* 2: 1–14, 2014.

Wang JW. Presynaptic modulation of early olfactory processing in Drosophila. *Dev Neurobiol* 72: 87–99, 2012.

Weiger WA, **Ma PM**. Serotonin-containing neurons in lobsters: origins and characterization of inhibitory postsynaptic potentials. *J Neurophysiol* 69: 2003–2014, 1993.

Wilson RI, **Laurent G**. Role of GABAergic inhibition in shaping odor-evoked spatiotemporal patterns in the Drosophila antennal lobe. *J Neurosci* 25: 9069–9079, 2005.

Wilson RI, **Turner GC**, **Laurent G**. Transformation of olfactory representations in the Drosophila antennal lobe. *Science* 303: 366–370, 2004.

Witz P, **Amlaiky N**, **Plassat JL**, **Maroteaux L**, **Borrelli E**, **Hen R**. Cloning and characterization of a Drosophila serotonin receptor that activates adenylate cyclase. *Proc Natl Acad Sci U S A* 87: 8940–8944, 1990.

Wu M, **Nern A**, **Williamson WR**, **Morimoto MM**, **Reiser MB**, **Card GM**, **Rubin GM**. Visual projection neurons in the lobula link feature detection to distinct behavioral programs. *Elife* 5, 2016.

Yaksi E, **Wilson RI**. Electrical coupling between olfactory glomeruli. *Neuron* 67: 1034–1047, 2010.

Yao Z, **Scott K**. Serotonergic neurons translate taste detection into internal nutrient regulation. *Neuron* 110: 1036–1050.e7, 2022.

Yuan Q, **Lin F**, **Zheng X**, **Sehgal A**. Serotonin modulates circadian entrainment in Drosophila. *Neuron* 47: 115–127, 2005.

Zhang X, **Gaudry Q**. Functional integration of a serotonergic neuron in the Drosophila antennal lobe. *Elife* 5, 2016.

Zhu Y. The Drosophila visual system: From neural circuits to behavior: From neural circuits to behavior. *Cell Adh Migr* 7: 333–344, 2013.